CHAPTER 1

INTRODUCTION

In the last decades, we have been observed a dynamic growth in the number of research works conducted in the region of cerebral cancer diagnosis. Many university centres are focused on the issue because of the fact that cerebral cancer is spreading among the world population. For example in India, the International Agency for Research on Cancer estimated indirectly that about 635 000 people died from cancer in 2008, representing about 8% of all estimated global cancer deaths and about 6% of all deaths in India [1].The absolute number of cancer deaths in India is projected to increase because of population growth and increasing life expectancy. Rates of cancer deaths are expected to rise, particularly, from increases in the age-specific cancer risks of tobacco smoking, which increase the incidence of several types of cancer. About three-quarters of Indians live in rural areas. Most deaths in India (and in most low-income or middle-income countries) occur at home and without medical attention. Due to its negative effects on affected people, the cancer diseases constitutes a high burden on national economy and a source of suffering for the family as well as the society.

Data regarding frequencies of various primary brain tumors (diagnosed according to the World Health Organization (WHO) classification), in 3936 pediatric patients (<18 yrs of age), was collected from seven tertiary care hospitals in India.

The most common primary pediatric brain tumors were astrocytic tumors (34.7%), followed by medulloblastoma and supratentorial primitive neuro-ectodermal tumors (22.4%), craniopharyngiomas (10.2%) and ependymal tumors (9.8%). The most common astrocytic tumor was pilocytic astrocytoma. In comparison to adults, oligodendrogliomas and lymphomas were rare in children [2].

Magnetic Resonance Imaging (MRI) has become a widely used method of high quality medical imaging, especially in brain imaging where MRI's soft tissue contrast and noninvasiveness is a clear advantage. MRI provide an unparallel view inside the human body. MRI reveals which parts of the brain are active in certain tasks with a spatial resolution of 2-5

millimetres, which is superior to any of the other non-invasive techniques in cognitive neuroscience. This means that places of activity in the brain that are as close as 2-5 millimetres apart in the brain can still be distinguished from each other. The temporal resolution (the minimal distance in time between two data points that can still be distinguished), however, is relatively poor (5-8 seconds) .Reliable and fast detection and classification of brain cancer is of major technical and economical importance for doctors

To start with, some of the principles underlying MRI will be considered. How is the MRI image obtained? This will be explained in the first section of this report. In cognitive neuroscience, MRI is used to indirectly infer the functional activity of the brain, in which case it is referred to as functional Magnetic Resonance Imaging (fMRI). How neural activation leads to an fMRI signal will be discussed in the second section of this report. In the third section of this report, attention will be focused towards issues relating to the different kinds of experimental design that can be used in fMRI experiments. The fourth section of this report will be devoted to the different steps of analysing MRI datasets.

To identify a tumor, a patient will undergo several tests. Most commonly Computed Tomography (CT) and Magnetic Resonance Imaging (MRI) are used to locate brain tumor. The information obtained will influence the treatment a patient will receive. Perhaps the most widely used clinical diagnostic and research technique is MRI. It's an efficient medical imagery tool that has different methods (T1,T2, ARM, …) having each particular property and an effective way that enables to clarify the various tissues and to obtain a 2D, 3D and even 4D sight (3D+T) of a part of the body, in particular of the brain. It's based on the principal of nuclear magnetic resonance (NMR). Due to various sequences various tissues with high contrast can be observed.

Wavelet transform is an effective tool for feature extraction, because they allow analysis of images at various levels of resolution. This technique requires large storage and is computationally more expensive. Hence an alternative method for dimension reduction scheme is used. In order to reduce the feature vector dimension and increase the discriminative power, the principal component analysis (PCA) has been used. Principal component analysis is appealing since it effectively reduces the dimensionality of the data and therefore reduces the computational cost of analyzing new data.

Several methods such as linear or quadratic discriminant analysis and k-nearest- neighbor techniques are used to classify MR images. All these classifiers are conceptually straightforward way of approximating any real valued or discrete valued classification function. However, these methods are too slow and less accurate to use for many applications when dealing with large amounts of data. Latest development in data classification research has focused more on kernel based techniques such as support vector machine (SVM) and relevance vector machine (RVM). Support vector machines are a state of the art pattern recognition technique grown up from statistical learning theory. RVM has a probabilistic Bayesian learning framework and has good generalization capability. In the last few years SVM and RVM have shown excellent performance in many real-world applications including medical field. The motivation behind this work is to develop a machine classification process using SVM and RVM for MRI volume classification and evaluating the performance of classifiers.

CHAPTER 2

BASICS OF MRI

Magnetic Resonance Imaging, or MRI, typically measures the response of hydrogen molecules to a perturbation while in a magnetic field. Explaining the physics of MRI in full detail would be beyond the scope of this report. However, some basic knowledge of the principles is required to fully understand the subsequent sections.

There are four basic steps involved in measuring the MRI signal. The first step is to place the brain in a magnetic field. The second step is the application of a brief radiofrequency (RF) pulse and the third step is measuring the relaxation [5]. The fourth step is transforming this signal to obtain a 3-dimensional MRI image [3] [4] [6].Each of these steps will be considered in turn, concluding with a discussion of the pulse cycles that are commonly used.

2.1 The brain in a magnetic field

The first step to measuring an MRI signal is to place the brain in a magnetic field. This will cause the atomic nuclei to align with the magnetic field. This occurs to all nuclei that are electrically charged and spin around their axis. Of the many types of nuclei in the brain, it is the hydrogen nucleus that is most commonly measured in MRI [3] [4] [6].This is because hydrogen nuclei are abundant in the human brain and give a strong MRI signal.

Hydrogen nuclei are positively charged particles that spin around their axis. When an electrically charged particle moves, it produces a magnetic field. This magnetic field can be represented as a vector (a mathematical entity with both an amplitude and a direction).Generally, a vector is mathematically depicted as an arrow where the length of the arrow represents the amplitude of the vector and the direction in which the arrow is pointing reflects the direction of the vector. Since each hydrogen nucleus produces a magnetic field, which can be represented as a vector, this equals saying that each hydrogen nucleus in the brain can be seen as a vector with the vector representing the strength and direction of the magnetic field of the hydrogen nucleus produced by its spinning around its axis. This vector is also known as the Magnetic Dipole Moment (MDM) [3] [4] [5] [6].

Before the brain is placed in a magnetic field, the MDM.s of each hydrogen nucleus points in a random direction the nuclei are not aligned. When the brain is placed in a magnetic field, two things happen simultaneously [3] [4] [6].

Firstly, the MDM.s of many of the hydrogen nuclei aligns themselves in the direction of the main magnetic field. How many of the MDM.s align themselves in the direction of the main magnetic field depends on the strength of this magnetic field. The stronger the magnetic field, the higher the percentage of the MDM.s that align themselves to the magnetic field [3] [4] [6].Secondly, when the brain is placed in a magnetic field the MDM.s of the hydrogen nuclei start to precess (see Fig. 1.1). The frequency of this precession depends first of all on the type of nucleus. This means that the MDM of a hydrogen nucleus will have a different frequency of precession from, for instance, the MDM of sodium nuclei in a certain magnetic field. Second of all, the frequency of precession depends on the strength of the magnetic field. The frequency of precession is directly proportional to the strength of the magnetic field, so the stronger the magnetic field the higher the frequency of precession. For example, in a magnetic field of 1.5 Tesla the frequency of precession for the MDM.s of hydrogen nuclei will be 64 MHz (64000000 revolutions per second) and in a magnetic field of 3 Tesla the frequency of precession will be 128 MHz [5] [6].

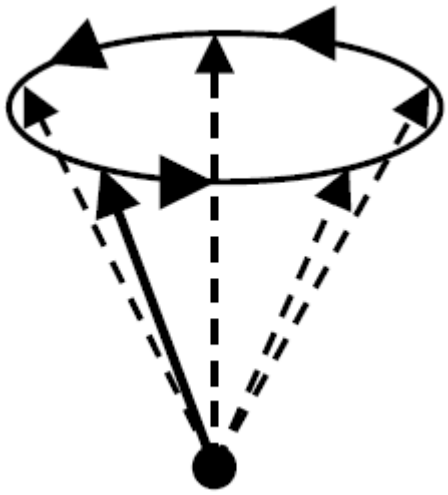

Fig. 2.1: Precession of the MDM; the .tail. is stationary while the .top. moves around in a circular motion.

2.2 Application of the radiofrequency pulse

The second step when measuring the MRI signal is the brief application of the radiofrequency pulse. The Radio Frequency (RF) pulse is typically an electromagnetic wave resulting from the brief application of an alternating current perpendicular to the direction of the main magnetic field, otherwise known as a 90^0 RF-pulse [3] [4] [6].The ultimate goal of this 90^0 RF-pulse is to tip the MDM.s of the hydrogen nuclei. Conventionally, the direction along the main magnetic field is referred to as the z-axis. The 90^0 RF-pulse then basically tips the MDM.s in the x-y plane (see fig. 1.2). This will only work if the frequency of the RF- pulse equals the frequency of the precession of the MDM.s. Because the MDM.s of the hydrogen nuclei have their own specific frequency of precession in a given magnetic field, it is possible to selectively tip the MDM.s of the hydrogen nuclei [3] [4] [6].

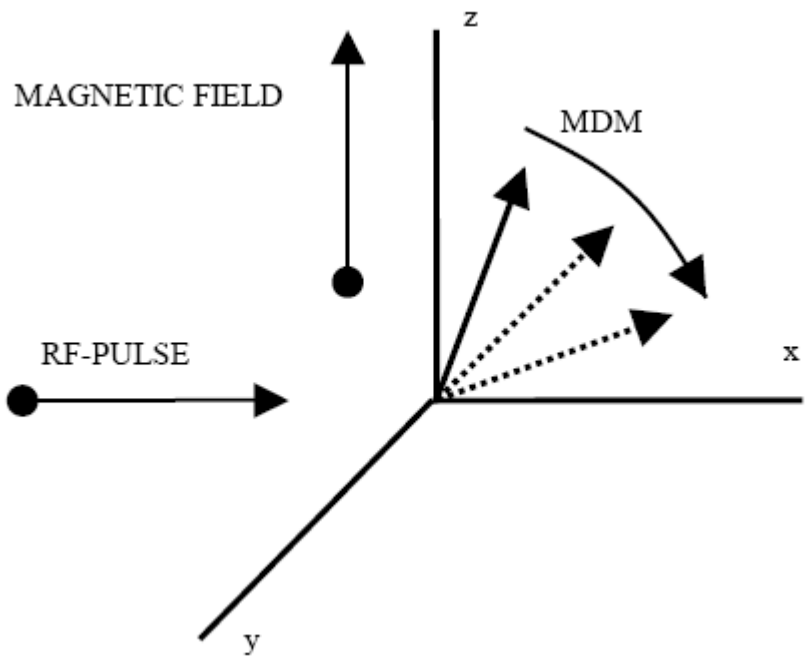

Fig 2.2: .Tipping. of an MDM into the x-y plane during application of the RF-pulse.

After the MDM.s of the hydrogen nuclei are .tipped., the 90^0 RF-pulse is terminated and the MDM.s return to their original orientation. This returning to the original orientation is known as relaxation [3] [4] [6].

2.3 Relaxation

After the 90^0 RF-pulse is terminated, the MDM.s of the hydrogen nuclei will return from their .tipped. state to their original lower energy state of being aligned in the direction of the magnetic field [3] [4] [6].Basically, the RF-pulse poured energy into the system and this energy is released when the MDM.s return to their original state. This release of energy is known as relaxation and is the signal that is measured during MRI [3] [4] [6].

The MDM of a hydrogen nucleus can be broken down into two components. One component of the MDM is the amplitude in the z-axis. The other component of the MDM is the amplitude in the x-y plane [3] [4] [6].Before application of the RF-pulse the amplitude in the z-axis is maximal while the amplitude in the x-y plane is zero. Just after application of the RF-pulse the amplitude in the z-axis is zero while the amplitude in the x-y plane is maximal. During relaxation the amplitude in the z-axis will slowly increase while the amplitude in the x-y plane slowly decreases. Therefore, the relaxation of the MDM.s of the hydrogen nuclei has two components; firstly, a re-growth along the z-axis and secondly, a decay in the x-y plane. The re-growth along the z-axis of the MDM.s is referred to as T1 relaxation. The decay in the x-y plane of the MDM.s is referred to as T2 relaxation [3] [4] [6].

2.4 When it all comes together

The application of the 90^0 RF-pulse and the measuring of the energy released during relaxation is repeated over a vast amount of times in a typical MRI experiment.

Different tissues in the brain have different T1 and T2 relaxation rates [3] [4] [6].This means that at each moment after termination of the RF-pulse, the amplitude of the MDM.s of the hydrogen nuclei in the z-axis and the amplitude of the MDM.s in the x-y plane will be different for different tissues. If now the MRI signal is measured at a point after termination of the RF-pulse where either the relative difference between the amplitudes of the MDM.s of the hydrogen nuclei of different tissues in the z-axis is maximized or the relative difference between the amplitudes of the MDM.s of different tissues in the x-y plane is maximized a maximum contrast between different tissues will be obtained [3] [4] [6].

At first, it sounds a bit counterintuitive that not the absolute difference in amplitude is maximized but instead the relative difference between the amplitudes is maximized. An analogy might clarify things a bit. Imagine a person A who makes 20,000 dollars a year and a person B who makes 22,000 dollars a year. The absolute difference is 2,000 dollars but the relative difference is quite small (10%). As a consequence, person B doesn't really feel a lot richer than person A because the contrast between the two incomes is not very big. If now, on the other hand, person A makes 3,000 dollars a year and person B makes 4,700 dollars a year, even though the absolute difference is now smaller (1,700 dollars), the relative difference is a lot bigger. In the second case, even though the absolute difference is smaller, the relative difference is a lot larger and person B ends up feeling a lot better off than person A because the contrast between the two incomes is now a lot bigger. To return to contrasts between different tissues in the brain, it can now be seen that to maximize contrast between different tissues the MRI signal must be measured at a time when the relative difference in amplitudes of the MDM.s is maximized and not the absolute difference.

When the MRI signal is measured at a point when the ratio of the amplitudes of MDM.s of different tissues in the z-axis is maximized, the signal is known as a T1 weighted signal. Alternatively, when the MRI signal is measured at a point when the ratio of the amplitudes of the MDM.s of different tissues in the x-y plane is maximized, the signal is known as a T2 weighted signal [3] [4] [6].By changing certain scanner parameters either a T1 weighted signal or a T2 weighted signal can be acquired [3] [4] [6].When the time from RF-pulse to measurement of the signal (TE) is kept short, while at the same time the time between two successive RFpulses (TR) is also kept short, the difference in T1 for the different tissues is maximized and the acquired scan is called a T1 weighted scan. T1 weighted scans are also known as anatomical scans, because they particularly show good contrast between grey and white matter. On the other hand, when the TE is long while at the same time the TR is also long, the difference in T2 for the different tissues is maximized and the acquired scan is called a T2 weighted scan. T2 weighted scans are also known as pathological scans, because lesions appear very bright [5] [6].

2.5 T2* and the spin-echo pulse cycle

In the previous sections, it was implied that the decay of the MDM.s in the x-y plane after termination of the 90^0 RF-pulse equals the T2 relaxation signal. This is, however, a simplification and to really understand the use of MRI we will need to explain T2 in more detail. True T2 decay is actually a lot slower than the decay of the MDM.s in the x-y plane after termination of the 90^0 RF-pulse. The decay of the MDM.s in the x-y plane is more accurately described as T2* decay [3] [4] [6].So, the question remains; what is T2 decay?

The reason why the MDM.s decay in the x-y plane (the T2* signal) is essentially due to dephasing [3] [4] [6].Remember that the MDM.s of hydrogen nuclei in a magnetic field of a certain field strength all precess at the same frequency. However, before the application of the 90^0 RF-pulse, they are not precessing in the same phase. To clarify this, an analogy with a clock can be helpful. Imagine a number of clocks that are not synchronized. Even though the hands of the different clocks rotate at the same frequency (an hour lasts equally long for all clocks), at a given moment the times the clocks indicate are not the same i.e. the clocks are not in phase. When applied to the precession of the MDM.s in a magnetic field, this means that even though the MDM.s precess at the same frequency, they will each be at a different position in their cycle at a given point in time i.e. they are precessing in a different phase (see fig. 1.3) [5][6].

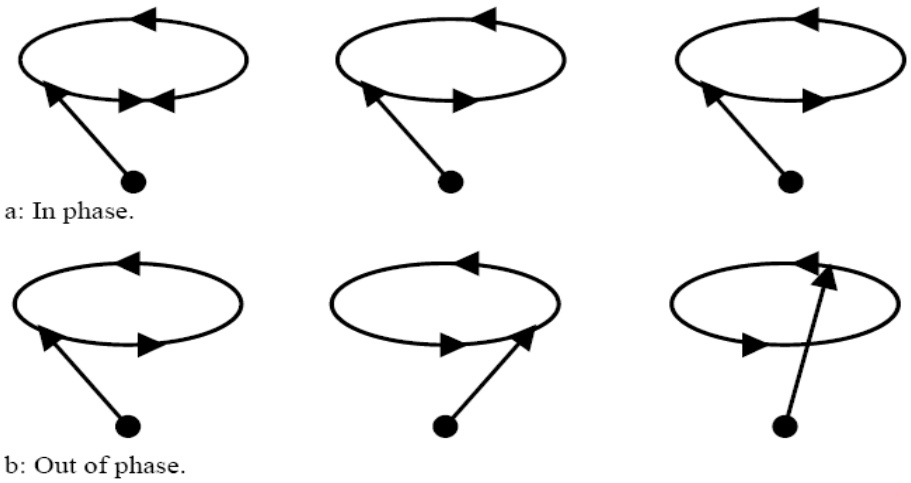

Fig 2.3: The top row displays one moment in the cycle of precession of 3 MDM.s that are in phase. The bottom row displays one moment in the cycle of precession of 3 MDM.s that are not in phase.

At the moment when the 90^0 RF-pulse is applied, the MDM.s are .tipped. in the x-y plane and are forced to precess in phase (as the brief RF-pulse .tips. all the MDM.s simultaneously). Now the MDM signals are additive and therefore result in a strong signal in the x-y plane. After termination of the 90^0 RF-pulse, however, the precession of the MDM.s will gradually dephase. The MDM signals are now no longer additive, but cancel each other out and the signal decays. This is the T2* decay [3] [4] [6]. There are two reasons why the MDM.s dephase after termination of the 90^0 RF-pulse and the signal decays [3] [4] [6].The first one is magnetic field inhomogeneity. The strength of the magnetic field is not uniform and since the frequency of precession of the MDM.s depends on the strength of the magnetic field it follows that different MDM.s will precess at a different frequency and therefore this precession will get out of phase. The second reason why the MDM.s dephase is because of spin-spin interaction[3] [4] [6].. Different hydrogen nuclei are surrounded by different other nuclei. These other nuclei affect the frequency of precession of the MDM of the hydrogen nuclei. The frequency of precession of each MDM.s will be differently affected by the surrounding nuclei. This, again, results in different frequencies of precession for different MDM.s and hence dephasing occurs [3] [4] [6].

To summarize, initially the precession of the MDM.s is dephased. When the 90^0 RFpulse is applied, the MDM.s are forced to precess in phase, resulting in a signal in the x-y plane. After termination of the 90^0 RF-pulse, the precession of the MDM.s will dephase again due to the inhomogeneities in the magnetic field and spin-spin interactions and the signal in the x-y plane decays. This is T2* decay.

The trick is that the dephasing due to the inhomogeneity of the magnetic field is correctable and by correcting for this source of dephasing the true T2 signal is obtained [3] [4] [6]. Directly after application of the 90^0 RF-pulse the precession of the MDM.s is in phase. This means that at a given time, all the MDM.s will be at the same point in their cycle of precession. After termination of the 90^0 RF-pulse the precession of the MDM.s will slowly dephase. Basically, at a given time, different MDM.s will not longer be at the same point in their cycle of precession. If an RF-pulse is now applied from the opposite direction (180^0) as the direction from which the original RF-pulse was applied (90^0), the direction of rotation of the precession of the MDM.s is reversed. After the same amount of time has elapsed following the 180^0 RF-pulse as

the amount of time between the 90^0 RF-pulse and the 180^0 RF-pulse, the MDM.s will be in phase again [3] [4] [6].

An analogy might, again, be helpful. Imagine two cars leaving from the same point in the same direction. One is moving at a speed of 100 km/h and the other one is moving at a speed of 80 km/h. After a while the faster car will be further away from the point of origin than the slower car. After, for example, half an hour both cars turn around and head towards the point of origin again. If both cars keep moving at their same respective speed, they will both arrive at the point of origin again at the same time. To relate this analogy back, directly after application of the 90^0 RF-pulse all the MDM.s are at the same point in their cycle of precession. After termination of the RF-pulse some MDM.s will rotate faster (have higher frequencies of precession) than others, the MDM.s dephase. After a while the 180^0 RF-pulse is applied and this makes the direction of precession of all the MDM.s reverse. The MDM.s, however, all keep their own frequency of precession and will arrive at their starting point (the point where they were directly after application of the 90^0 RF-pulse) in the cycle of precession at the same time, they will be in phase again.

The important thing is that the time between the 180^0 RF-pulse and measurement of the signal must be the same as the time between the 90^0 RF-pulse and the 180^0 RF-pulse. A measurement cycle where one 90^0 RF-pulse is followed by one or more 180^0 RF-pulses with a measurement after each 180^0 RF-pulse is known as a spin-echo pulse cycle. Even though the spin-echo pulse cycle corrects for the decay in the signal caused by the in homogeneities in the magnetic field, the signal still does eventually decay because of the de phasing due to spin-spin interactions. The decay is now, however, a lot slower and this is the true T2 decay [3] [4] [6].

CHAPTER 3

FROM NEURAL ACTIVATION TO THE fMRI SIGNAL

Besides looking at structural scans of the brain, MRI can also be used to look at functional activity of the brain, in which case it is referred to as functional Magnetic Resonance Imaging (fMRI). The type of scanning technique most commonly used to obtain fMRI images is Echo Planar Imaging (EPI), which is basically a technique that allows for fast measurement of the signal. The technique most commonly used in fMRI is the so-called BOLD (blood oxygenation level-dependent contrast) technique. The BOLD technique is based on the fact that, under normal circumstances, neuronal activity and haemodynamics (regulation of blood flow and oxygenation) are linked in the brain. In this section the relationship between neuronal activity and haemodynamics will be explained.

3.1 The T2* signal

As explained in the previous section, the amount of energy released by the hydrogen molecules after the termination of the RF-pulse gradually decays over time. The speed of this decay differs for different tissues and this makes the distinction between different types of tissue possible. One reason for the decay of the fMRI signal is the dephasing of the precession of the MDM.s of the hydrogen nuclei due to inhomogeneities in the magnetic field. The larger the inhomogeneity of the magnetic field, the faster the precessions of the MDM.s will dephase and the faster the fMRI signal decays. Since the fMRI signal is measured at a predetermined point in time after termination of the RF-pulse, the magnitude of the fMRI signal will be smaller at that time of measurement when the signal decays faster as compared to when the signal decays slower (see fig. 3.1). Therefore, the larger the inhomogeneity of the magnetic field, the smaller the fMRI signal at the time of measurement.

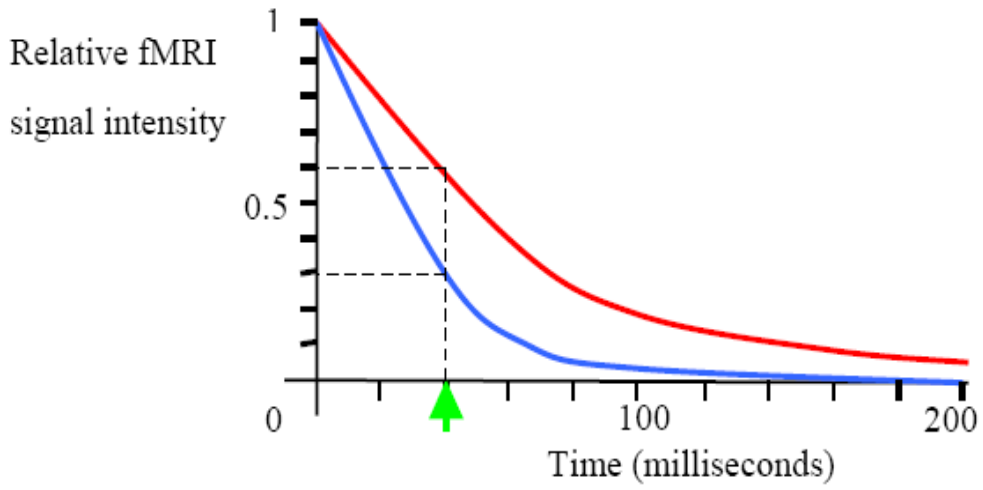

Fig. 3.1: Decay of the fMRI signal over time after termination of the RF-pulse. The blue curve represents the decay in fMRI signal in a magnetic field with a larger inhomogeneity. The red curve represents the decay in fMRI signal in a magnetic field with a smaller inhomogeneity. Therefore, the blue curve decays faster than the red curve. The green arrow indicates the point in time at which the signal intensity is measured. It can be seen that when the fMRI signal decays faster (the blue curve), the signal intensity at the moment of measurement is lower than when the fMRI signal decays slower (the red curve).

Usually, this inhomogeneity of the magnetic field is considered an artefact and through a process known as .shimming. every attempt is made to make the overall magnetic field as uniform as possible. However, even though great care is taken to make the overall magnetic field as uniform as possible, small local inhomogeneities in the magnetic field still occur. In the BOLD fMRI technique these little inhomogeneities are used to indirectly measure neuronal activity. Since the T2 signal is relatively insensitive to inhomogeneities in the magnetic field (remember from the previous section that the T2 signal is obtained by correcting for the effects of the inhomogeneity of the magnetic field) it follows that the signal most commonly measured in BOLD fMRI is the T2* signal.

The BOLD fMRI technique basically measures changes in the inhomogeneity of the magnetic field, which are a result of changes in the level of oxygen present in the blood (blood oxygenation).Deoxyhaemoglobin (red blood cells without an oxygen molecule attached to it) has magnetic properties and will cause an inhomogeneity in the magnetic field surrounding it.

Oxyhaemoglobin (red blood cells with an oxygen molecule attached to it) has hardly any magnetic properties and therefore has very little effect on the magnetic field surrounding it. Therefore, a high level of deoxyhaemoglobin in the blood will result in a greater field inhomogeneity and therefore in a decrease of the fMRI signal.

The function of the fMRI signal against time in response to a temporary increase in neuronal activity is known as the Haemodynamic Response Function (HRF). The HRF goes through three stages (see fig. 3.2).

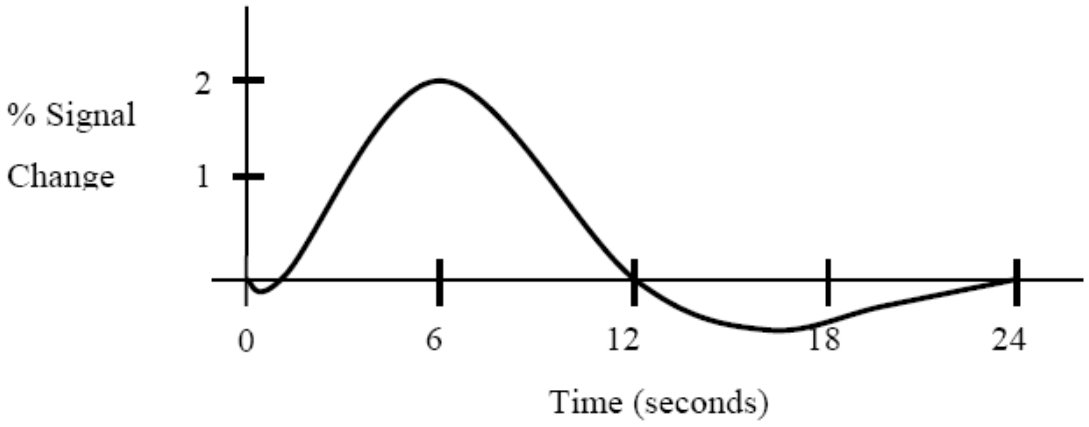

Fig 3.2: Time course of the HRF in response to a short-lasting increase in neuronal activity at time = 0.

The fMRI signal initially decreases, because the active neurons use oxygen thereby increasing the relative level of deoxyhaemoglobin in the blood. This decrease, however, is tiny and is not always found. Following this initial decrease, there is a large increase in the fMRI signal which reaches its maximum after approximately 6 seconds. This increase is due to a massive oversupply of oxygen-rich blood. There are two main hypotheses regarding the reason for this increase in blood flow. The first theory states that the increase in blood flow compensates for the oxygen being used by the active neurons. However, the supply in oxygen by the increase in blood flow is much larger than the amount of oxygen used by the active neurons. Instead, the increase in blood flow is proportional to the amount of glucose being used by the active neurons. Therefore, the second theory states that the increase in blood flow instead compensates for the amount of glucose being used by the neurons and not the amount of oxygen. In any case, the result of this oversupply of oxygen is a large decrease in the relative

level of deoxyhaemoglobin, which in turn causes the increase in the fMRI signal. Finally, the last stage of the HRF is a slow return to the normal level of deoxyhaemoglobin and a decay of the fMRI signal until it has reached its original baseline level after an initial undershoot after approximately 24 seconds.

It is important to note, first of all, that the BOLD fMRI signal is an indirect measure of the underlying neuronal activity and therefore strongly relies on the assumption that neuronal activity and haemodynamics are indeed linked. Secondly, the fMRI signal reflects the sum of the activity of a large group of neurons.This first of all means that an increase of the fMRI signal can both be caused by a large increase in activation of a small group of neurons and by a small increase in activation of a large group of neurons.Inherent, however, is also the deeper assumption that the neurons responsible for the same function will be grouped together in the brain. Thirdly, the BOLD fMRI signal is sensitive to contaminations of large veins in the brain . The relative decrease in deoxyhaemoglobin is larger in large veins than in small veins. This means that the maximum BOLD fMRI signal is often obtained in the large veins that can be a few millimeters away from the site of neural activation. Fourthly and related to the third point, the increase in blood flow (and the associated decrease in deoxyhaemoglobin) is not very specific to the area of neuronal activation. Usually, veins supply blood to a larger area of the brain than just the area of neuronal activation. This leads to spatial blurring, where the area that shows an increase in fMRI signal is larger than the area of neuronal activation. Finally, it is also important to note that the haemodynamic response is inherently much slower than the underlying neuronal activity. Basically, the fMRI signal can be seen as a smoothed function of the underlying neuronal activity . Because of this slowness of the haemodynamic response, fMRI has a relatively poor temporal resolution when compared to methods that more directly measure neuronal activity such as EEG . Note that this poor temporal resolution is inherent in the BOLD fMRI technique. While the spatial resolution might be improved by further technical innovations, the temporal resolution cannot be improved because of this inherent slowness of the haemodynamic response. The only way to improve the temporal resolution would be by measuring a more direct consequence of neuronal activity instead of the indirect consequence that is the haemodynamic response.

3.2 Optimizing the BOLD signal

As noted in the previous section, the magnitude of the BOLD effects measured during fMRI is very small. As Figure 3.2 depicts, a visual flash may result in a 2% signal change in the occipital cortex (the first cortical stage of visual processing). This low signal-to-noise is a severe limit on our statistical power (our ability to find real effects). Broadly speaking, there are three ways we can maximize statistical power. First, we can optimize the behavioral task used (e.g. using a block design), as discussed in the next section. Second, we can run very long fMRI sessions. Unfortunately, this is expensive and often results in participants feeling fatigue. A final method to maximize fMRI signal is to optimise the hardware, which we will discuss in this section. In practice, combining all three techniques is often required to detect subtle differences in the BOLD signal.

In particular, we identify four common practices that influence the BOLD signal. First, we discuss echo planar imaging and spiral imaging to collect images of the brain quickly. Next, we note that the strength of the T2* signal is greatly dependent on the echo time (TE). Third, we discuss the relationship between magnet field strength and signal. Fourth, we discuss how the matrix size, voxel size and receiver coil all critically influence the measured signal.

Optimal BOLD effects will be found when the echo time (TE) matches the T2* of blood. In theory, this means that the BOLD effect will be maximum with a TE of around 65ms at a field strength of 1.5T and around 40ms at 3.0T . In practice, most labs use slightly shorter echo times. This probably reflects a trade-off: by using a shorter TE, the BOLD effect in each image is reduced but more images are collected in a fixed amount of time. Therefore, while the signal in each sample may be reduced, the larger number of samples results in improved statistical power. Furthermore, the shorter TE can result in slightly reduced image distortion. In our own research, we use echo planar imaging with a TE of 60ms at 1.5T and a TE of 30ms at 3.0T.

As noted earlier, the numbers of hydrogen nuclei that align with the magnetic field depend directly on the field strength of the magnet (and the temperature of the sample, about 37 Celcius for the human brain). In a 1.5 Tesla, about 4.5 nuclei per million are aligned with the field than against the field, while at 3.0 Tesla the number of rises to about 9 nuclei per million. Therefore, at higher field strength, there is theoretically more signal to measure. Also, as noted in

the previous paragraph, the T2* of blood reduces at higher field strengths, allowing a shorter time to echo time. Therefore, we can collect images of the brain more rapidly at higher field strengths. Despite these advantages, higher field magnets also have limitations. First of all, increasing field strength drives up the installation and service cost for a MRI system, and higher field systems tend to be acoustically much louder (due to more powerful gradients required). Second, at higher field strengths inhomogeneity effects become more severe. Images from 3.0 Tesla magnets typically show much greater inhomogeity artefacts (with some regions of the brain appearing brighter than other regions), and exhibit regions of signal dropout than images from 1.5 Tesla systems. Clearly, studies in single individuals do reveal stronger fMRI signals with increasing field strength. However, images from higher field scanners may not necessarily yield better signal in group studies (as image distortion results in poor normalization of images, as discussed later) and may result in an inability to measure some regions of the brain (such as the medial temporal lobe and ventral frontal lobe).

With MRI scanning, one can trade-off image resolution for signal quality. By increasing the size of each voxel, we can effectively measuring more hydrogen nuclei. For example, consider axial slices where we have a 64x64 matrix (i.e. the image has 64 rows of pixels and 64 columns) with a field of view of 192x192mm (pixels are separated by 3mm in plane). If the distance between slices is 3mm, each voxel will measure 27mm^3, and it will require around 36 axial slices to cover the entire cortex and most of the cerebellum. On the other hand, if we collect images that are 5mm thick, each voxel will measure 45 mm^3, and we only need to collect around 22 slices. By collecting fewer slices, we can image the brain more rapidly, and get more samples of a given brain area. Another common technique to increase the speed of acquisition is to collect EPI data as axial or sagittal slices instead of coronal slices (as the brain is longest in the axial-posterior direction). Another issue is interference between slices: unless a gap is added between EPI slices, there will be some reduction in image quality due to the RF pulse saturating neighbouring slices along with the target slice. One simple technique to reduce this interference is to collect the data in an interleaved fashion: all the odd slices of an image are collected first (e.g. 1, 3...35) and then all the even slices (2, 4…36). This minimizes interference between slices and allows you to sample more nuclei than if a slice gap is employed.

CHAPTER 4

OVERVIEW OF MRI SCAN IMAGING SESSIONS

4.1 A brief introduction of fMRI

Functional MRI utilizes the magnetic properties of blood to analyze brain activity in specific areas. The technique is based on small changes in blood flow and is referred to as BOLD (Blood Oxygen Level-Dependent) imaging. During this procedure, induced variations in the ratio of oxygenated to deoxygenated blood in localized areas of the brain are imaged to generate fMRI results .

4.2 The fMRI procedure

There are three primary steps to an fMRI procedure: preparation, acquisition and processing.

4.2.1 Preparation:

The patient is given a detailed explanation of the procedure and carefully instructed on the chosen task in order to obtain the highest quality exam with the least amount of patient-induced motion. It is common to practice these tasks with the patient before the exam to assure the best results.

4.2.2 Acquisition:

The first step in the acquisition process is to collect routine 3D datasets. These will later be used as the anatomical data upon which the fMRI information will be mapped. Activity in specific regions of the brain is induced and controlled by a set of tasks called a paradigm. These tasks are performed by the patient during the BOLD imaging measurements. fMRI data collection is done in three sessions [7] described below .

fMRI Data collection:-

SESSION 1: Structural & functional sequences	**Duration**
1. Volunteer preparation / equipment adjustment	20:00
2. 3 plane localizer / Parallel imaging calibration	00:22
3. Axial T2 slices *(site specific duration)*	~01:19
4. Axial T2 Flair slices *(site specific duration)*	~ 02:25
5. Instructions / talk to volunteer	2:00
6. Face task	5:00
7. Instructions / talk to volunteer	2:00
8. Stop-signal task	16:00
9. B0 Map	00:40
10. 3D Sagittal ADNI MPRAGE (Long) Duration	09:17
Duration	**~60 min**

SESSION 2: Structural & functional sequences	**Duration**
1. Volunteer preparation / equipment adjustment	14:00
2. 3 plane localizer / Parallel imaging calibration	00:22
3. B0 Fieldmap	00:40
4. 3D Sagittal ADNI MPRAGE (Short)	02:23
5. Instructions / talk to volunteer	2:00
6. M&M Incentive Delay Task	11:06
7. Instructions / talk to volunteer	02:00

8. Global Cognition Assessment	05:00
9. Instructions / talk to volunteer	02:00
10. Breath Hold Task (optional)	05:40
11. DTI *(duration is heart-rate dependent)*	10:00
Duration	**~60 min**

OPTIONALSESSION 3: Structural & functional sequences	**Duration**
1. 3 plane localizer / Parallel imaging calibration	00:22
2. Despot	18:30
3. 3D Sagittal ADNI MPRAGE (Short)	02:23
Duration	**~22 min**

Important notes:

Please always try to run all of the tasks. In case you need to stop the scanning session earlier please skip the optional sessions / tasks first. We do not recommend running all sessions in one go as this is too tiring for the participant and has an impact on the data quality. If you have to do this please allow at least for a break between sessions. If you have scheduled two volunteers and you run both sessions on the same day please use the following scanning order which allows for breaks for the volunteer:

Volunteer 1: first session
Volunteer 2: first session
Volunteer 1: second session
Volunteer 2: second session

Paradigms, some of which are described below, differ based on the area of the brain being examined.

- **Motor Tasks:** The easiest paradigm to implement is a motor task. One version of this paradigm is finger tapping where the patient is asked to touch the thumb of one hand to each of the fingers during the activation portion of the data collection. Motor tasks are often implemented in presurgical planning to assess the effects of lesions close to the motor strip and to help improve the surgical outcome.
- **Auditory Tasks:** These tasks can involve rhyming or word generation and may require the patient to speak specific words or phrases during the active portion of the exam. This paradigm allows the clinician to visualize a lesion's proximity and effect on Broca's area, a key area of the brain associated with language, speech and comprehension.
- **Face Tasks:** In this task volunteers are asked to passively watch video clips presenting faces with neural and angry expressions as well as control non-biological motion stimuli (concentric circles). After scanning a short recognition test is performed outside the scanner with 5 static pictures extracted from the movies. The pictures are presented sequentially, each with the question: "Have you seen this object while you were in the scanner?" The volunteers are NOT informed that a recognition test will be performed after scanning.
- **Stop Signal Tasks:** The main principle of this task is to respond to regular presented visual go stimuli (go trials) but to withhold the motor response to the go stimulus when it is followed unpredictably by a stop-signal (stop trials). This task yields an estimate of a subject's stop-signal reaction time (SSRT). The SSRT is thought to be directly reflective of the central inhibitory mechanism.
- **MID (M&M Incentive Delay) Task:** This task is a reaction time task - it tests how quickly the subject can react and pull the trigger to hit a target (with left or right index finger) that only appears for a short time on the left or right of the screen. If the subject can hit the target, they will score points. The subject can tell where the target will appear and how many points they can win by the symbol they see on the screen before each trial. A triangle means no points, a circle with a line means 2 points and a circle with three lines means 10 points. Responding too early or too late will result in a loss. The task lasts 11 minutes and is adaptive - the maximum that can be won is <200 points.The subjects

receive 1 M&M (or similar chocolates/sweets) for every 5 points to enhance motivation during the task.

- **Visual paradigms:** Visual paradigms can be implemented when video projection systems are integrated into the examination. This type of paradigm can vary significantly but normally requires the patient to focus on specific images or projections during the examination. Examining the visual cortex in this way provides additional information that can assist the surgeon with minimizing negative surgical effects on vision when removing lesions in this area.
- **Breath Hold Task (Paced Expiration Breath Hold Task):** This task uses visual instructions to pace their breathing in a regular rhythm for 40 seconds (breathing in for 4 seconds and out for 4 seconds), followed by holding their breath *on expiration* for a short periods of 20 seconds. This cycle is then repeated five times, ending on paced breathing to give a total task length of 5 minutes 40 seconds. This task uses the small build up of carbon dioxide to assess vascular responsivity in each participant and which differs between participants. This task is optional but we would like to ask all sites to run it as these data can be used to calibrate the bold response and more accurately measure neural responses from all our other tasks.
- **Global Cognition Assessment Task:** Cognitive activation paradigms can be very complex and can include stimuli to examine areas of thought and reasoning or even pain and fear. These paradigms are normally confined to the realm of research but offer a clinical benefit in understanding the anatomic areas associated with processes such as learning, memory and decision making.

This task is composed by the following brief tasks:

1. passive viewing of a flashing checkerboard (20 trials),
2. pressing three times the left button with the left index finger according to visual instructions (5 trials),
3. pressing three times the right button with the right index finger according to visual instruction (5 trials),
4. pressing three times the left button with the left index finger according to auditory instruction (5 trials),

5. pressing three times the right button with the right index finger according to auditory instruction (5 trials),
6. reading silently short visual sentences (10 trials),
7. listening to short sentences (10 trials),
8. solving silently visual subtraction problems (10 trials),
9. solving silently auditory subtraction problems (10 trials).

4.2.3 Processing:

After data collection, a statistical evaluation (t-test) is used to generate BOLD maps that are combined with routine 3D imaging datasets such as MPRAGE. The combined data can then be used as a neuronavigational roadmap for use in pre surgical planning or treatment assessment.

CHAPTER 5

ANALYSIS OF MRI SCAN

In a typical fMRI experiment, a measurement of the entire brain, known as a volume is collected every 2 to 4 seconds, resulting in hundreds of collected brain volumes per experiment for each subject. This means that the HRF is sampled at many different points in time. Every volume consists of a number of 3D slices (or slabs). These slices are typically a few millimetres thick. Each slice consists of a number of voxels (a 3D data points) and each voxel represents a data point on the HRF. An fMRI voxel of size $\sim 3 \times 3 \times 5 mm^3$ contains millions of neurons. When neurons in an area become active, blood rich in oxygen flows to the area. The source of the fMRI signal is the difference in the magnetic properties of oxygenated blood from deoxygenated blood. The measured hemodynamic response due to the BOLD effect, which is the neurovascular response to brain activity, lags behind the neuronal activity by approximately 3–6s. Higher static magnetic field (B0) strengths and more sophisticated MRI pulse sequences are often used to increase the signal-to-noise ratio (SNR). The acquired images are then preprocessed to correct for head motion, compensate for signal dropouts and magnetic field distortions, and apply spatial smoothing.

5.1 SIGNAL ACQUISITION

Conventional MRI has been a slow imaging modality where increases in imaging speed result in signal losses. The reason is that the MR signal is derived from the on version of tissue magnetization to a radio signal, and the magnetization recovers rather slowly. This had limited the possibility of implementing a real-time MRI. Fortunately, over the last 20 years technical advances in imaging have enabled substantial reduction in acquisition time. The most significant speed advance came with the development of echo-planar imaging (EPI). EPI is capable of imaging the entire brain in 1–2 s. At this sampling rate, fMRI can accurately follow the time course of brain activation.

In EPI, one 3D slice is collected at a time. Alongside the EPI volumes that display areas of the brain that are active in a given task (functional activity) often a high resolution T1 or T2

anatomical volume is also obtained. This anatomical volume is used for spatial localization of the areas of the brain that are active in a given task.

In a traditional fMRI experiment, images are reconstructed offline only after the experiment has been completed. Real-time fMRI, on which fMRI-BCI is based, requires the simultaneous reconstruction of the images with the acquisition of the MR signal. Cox's group reported the first implementation of a real-time fMRI system using a whole body 3T scanner (Bruker Instruments) . In their implementation, the analog signal from the signal acquisition system was sent to a workstation for analog-to-digital conversion and image reconstruction. This can also be implemented by modifying the Siemens MR scanner's image reconstruction software to allow online reconstruction of whole-brain images at the end of every repetition time (TR) and storage of these images in a pre-specified folder to be immediately retrieved for further processing, analysis, and feedback by the fMRI-BCI system. The online image reconstruction software program is written in C++ based on the image reconstruction environment (ICE) provided by Siemens. The RT Export system runs both on the 1.5 T (Vision) and 3 T (TIM Trio) Siemens scanners.

Many factors influencing signal acquisition have important consequences for real-time performance of fMRI-BCI: static magnetic field (B0) strength, spatial resolution, temporal resolution, echo time, and magnetic field inhomogeneities. Although high spatial resolution is desired, increasing the spatial resolution decreases the SNR and increases the acquisition time, and hence a compromise needs to be made among these variables. Commonly in fMRI-BCI, 64x64 image matrices resulting in 3–4 mm in-plane resolution, and slice thickness of around 5 mm are used. For online processing after image acquisition, spatial filtering or averaging across an ROI helps improve SNR. Reduced spatial resolution could be beneficial, compensating for head motion, data complexity, and inter-subject variability. A TR of 1,500 ms has been used in real-time fMRI with single-shot EPI. It is advisable that fMRI-BCI studies choose the echo time (TE) close to the relaxation time ($T2*$) of the gray matter in the brain to maximize functional sensitivity. This value is about 70 ms at 1.5 T and 45 ms at 3 T.

At the interface between tissue and air in the brain, in areas such as the orbitofrontal cortex and temporal pole, a significant change in the local magnetic field is present over a short

distance. Artifacts such as signal dropouts and geometric distortions (local shifts and compressions in the image) caused by magnetic field inhomogeneities potentially affect the performance of fMRI-BCI. Several methods have been developed for reducing susceptibility-related signal losses in fMRI Weiskopf et al. developed a theory supported by experimental evidence showing that susceptibility-induced gradients in the EPI readout direction cause severe signal losses. They have proposed a model to simulate EPI dropouts to make informed choice of scan parameters depending on the field inhomogenieties in a region. Based on this insight, they developed an optimized EPI sequence for maximal BOLD sensitivity using a specific combination of an increased spatial resolution in the readout direction and a reduced echo time. We foresee the real-time adaptation of such techniques for fMRI-BCI applications.

The signal analysis subsystem performs statistical analysis and generates functional maps using any of the following methods: subtraction of active and rest conditions, correlation analysis, multiple regression, general linear model (GLM), and pattern classification. Feedback can be presented to the subject by different modalities, including acoustic and visual, and with a variety of visualization methods, such as functional maps, continuously updated curves of the mean activity in one or more selected regions of interest (ROI), varying activity levels in one or more ROIs using a graphical thermometer, and augmented interfaces such as virtual reality (VR). Feedback is presented at an interval that depends on the time involved for image acquisition and processing, based on the computational resources available and the efficiency of the algorithms with which they are implemented, thus directly affecting the performance of the system. A short interval is critical for learning voluntary control of brain activity.

5.2 SIGNAL PREPROCESSING

After obtaining the EPI data from the scanner, a number of stages of analysis must be performed on the dataset to finally end up with a map that displays the regions with significant functional activity. These stages can roughly be subdivided in a stage where the data is temporally adjusted, stages where the data is spatially adjusted and a stage of statistical analysis. The stage where the data is temporally adjusted is known as slice timing correction. The stages where the data is spatially adjusted are spatial realignment, spatial normalization and spatial smoothing. Methods of signal preprocessing can be head motion artifact correction, respiratory

and cardiac artifact correction, and spatial smoothing. The last stage is the stage of statistical analysis [8].Each of these stages and their consequences for data interpretation will be considered separately in the following paragraphs.

5.2.1 Slice timing correction

In EPI every 3D volume of the entire brain consists of a number of 3D slices and these slices are each collected at a slightly different time. However, during the statistical analysis the assumption is made that the entire volume is collected at one point in time, so each voxel in a volume is assumed to represent the same moment in time. The result is that it might seem as though the same change in the HRF starts at an earlier time for slices that are acquired later in time than for slices that are acquired earlier in time (see fig. 5.1).

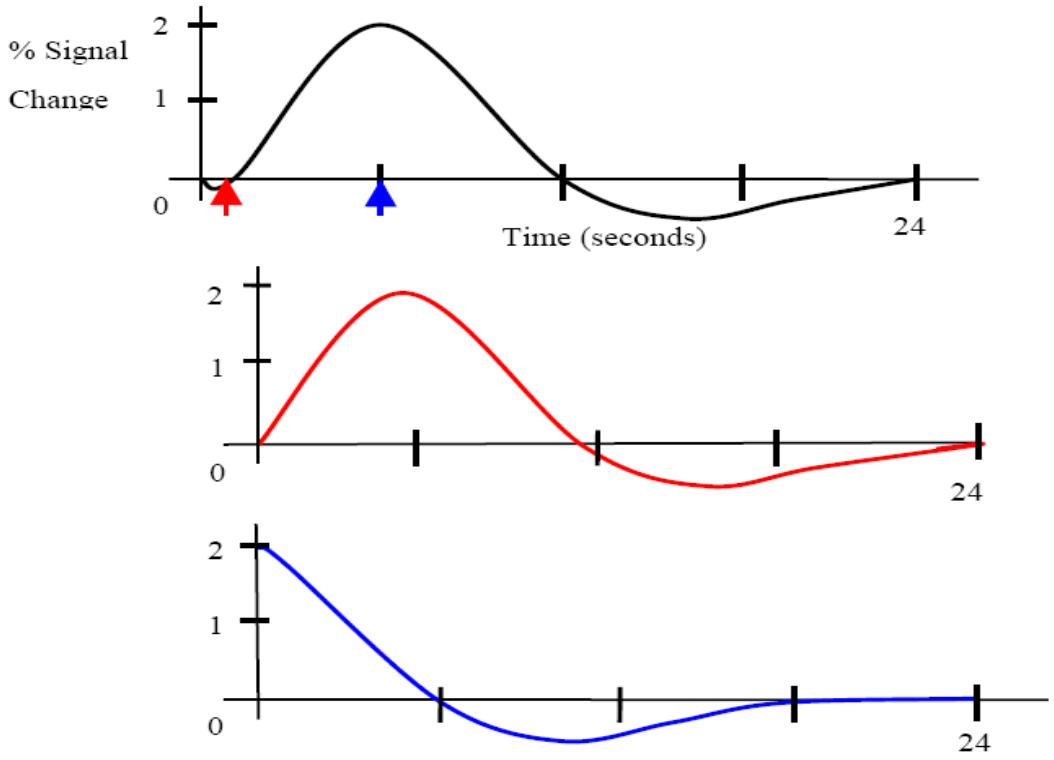

Fig. 5.1: The HRF over time. The red arrow represents the time of acquisition for an early slice in the volume, the blue arrow represents the time of acquisition for a later slice in the volume. When the assumption is made that the entire volume is collected at one point in time (as is done in the statistical analysis), it seems as though the HRF begins earlier for the slice that is acquired at a later time (blue curve) than for the slice that is collected at an earlier time (red curve).

To solve this, the individual slices of a volume must be adjusted in the temporal domain. This is done by performing a temporal correction for the differences in acquisition time between the slices. This is referred to as slice timing correction [6].First, a decision must be made as to which slice is going to be the reference slice. In other words, which time of acquisition of is going to be taken as the point in time that the entire volume of the brain was collected? Usually, either the first slice or the middle slice of the image of the brain is taken as the reference slice. After a certain slice has been chosen as the reference slice, all the other slices in the image of the entire volume of the brain are shifted in time by method of interpolation. The slices of a volume that are collected earlier in time than the reference slice are weighted with the same slice in the subsequent volume. The slices of a volume that are collected later in time than the reference slice are weighted with the same slice from the previous volume. For example, if a volume consists of 10 slices with the fifth slice being the reference slice, the second slice would be weighted with the second slice of the subsequent volume and the eighth slice would be weighted with the eighth slice from the previous volume. The reference slice is the only slice that is not shifted in time. The end result is that each voxel in each slice will approximately have the value that they would have had, had they been obtained at the same point in time as the voxels in the reference slice. In other words, the same change in the HRF now starts at the same time for each voxel in each slice in a volume [6].

Which slice to choose as the reference slice depends on where in the brain interesting activations are expected to occur. As the difference in time of the phase shifted slice from the reference slice increases, the artefacts introduced by this phase shift also increase. This is basically because the interpolation method used to shift the slices of a volume in time is not perfect. The further in time slices have to be shifted, the larger the errors in the interpolation. Therefore, it is important to choose the reference slice as close as possible to the region where the interesting activations are expected to occur, so that the interesting activations are not confounded by errors of interpolation.

5.2.2 Spatial realignment

During an fMRI experiment, hundreds of EPI 3D brain volumes are collected per subject in a single time series. Even though subjects are usually instructed to move as little as possible

inside the scanner, some head movement is unavoidable. The main result of head movements is that the same voxel does not to represent the same location in the brain throughout time [9]. The statistical analysis, however, assumes that the same voxel does represent the same location in the brain throughout time.

When the same voxel over time .moves. from a location of the brain with a low fMRI signal to a location of the brain with a higher fMRI signal, while the statistical analysis assumes that this voxel represents the same location in the brain throughout time, it appears as though there was an increase in the fMRI signal for that voxel over time while in reality there was no increase in the fMRI signal. This has two potential consequences. Firstly, when movements are correlated with task performance, for example, if the head movement always occurs at a certain time after stimulus presentation, these false increases in the fMRI signal ultimately appear as false activations in the brain after the statistical analysis [9].Secondly, even when these intensity changes in the voxel caused by the movement of the head are not correlated with task performance they will add to the noise in the signal, thereby worsening the signal to noise ratio, which decreases the statistical power [9].

The removal of movement effects is done for each subject separately and is referred to as spatial realignment or, alternatively, as within modality image coregistration [9].One brain volume (usually the first image in the time series) is taken as the reference volume. All the other volumes in the same time series are repositioned until they are in the same position as the reference volume. This repositioning is done using 6 parameters; x-translation, y-translation, z-translation, rotation around the x-axis, rotation around the y-axis and rotation around the z- axis (these transforms are discussed in more detail in the next section). Only the position of the brain is changed and not the size or shape. This repositioning treats the head as a rigid object and is therefore also known as a rigid body transformation.

For this realignment SPM2 uses a minimization algorithm for the least mean square difference between the volumes in the time series and the reference volume. This means that for each volume the squared difference between the volume in the time series and the reference volume is minimized (see Fig 5.2). The new value of the fMRI signal for a voxel after the

realignment is estimated by interpolation from the values of the fMRI signal of neighbouring voxels [9].

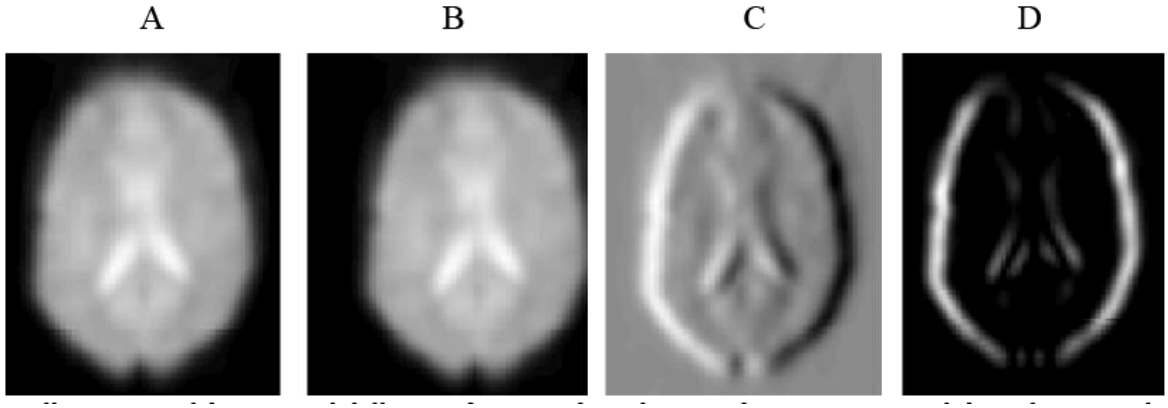

Fig 5.2: Illustration of the squared difference between the volume in the time series and the reference volume. **A**: The reference volume. **B**: the volume that has to be adjusted due to head movement. **C**: The difference between A and B. **D**: The squared difference(variance) between A and B.

It should be noted that realignment not only adjusts for actual head movement, but also for apparent movement. As the fMRI scanner heats up during a session it appears as though the head drifts slightly. This is an artefact arising from the scanner and is also corrected for by realignment.

Unfortunately, there are a number of limitations of realignment. The first limitation is that, when the head movements are too large, the minimization algorithm might get stuck in a local minimum [9].Usually, the data of subjects with movements that are too large will have to be removed. The second limitation is that the brain is not rigid. Heart-beat and respiration cause variations in shape and size of the brain. Usually, this source of movement is ignored [9].The third limitation is that even perfect realignment will not remove all movement related variance [9].The problem is that, in case of a movement, the image not only moves, but also fundamentally changes. The time it takes to acquire one image of the brain is usually shorter than the time it takes for the hydrogen nuclei to relax after the radiofrequency pulse. This means that, by the time the next radiofrequency pulse occurs, there is still a residual effect from the previous radiofrequency pulse on the hydrogen nuclei. This is not really a problem when the head does not move in the scanner, because in that case the residual effect from the previous

radiofrequency pulse is predictable. However, when the head does move the residual effect from the previous radiofrequency pulse on the hydrogen nuclei becomes unpredictable [9].One way to remove all movement related variance is to use a linear regression to remove any variance in the signal that is correlated with both movements during the present scan and movements during the preceding scan. However, when the movements are correlated with task performance, there is a risk of accidental removal of interesting activations [9] .The fourth limitation of realignment is that a movement also changes the overall magnetic field. Remember from the second section in this report that inhomogeneities in the magnetic field result in a decrease in the fMRI signal. Through a process known as shimming. every attempt is made to make the overall magnetic field as uniform as possible. However, when the head moves the overall magnetic field changes. Shimming is usually only done at the beginning of a scanning session and head movements therefore create new inhomogeneities in the overall magnetic field, leading to the overall magnetic field no longer being uniform and consequently to loss of signal in some areas of the brain. The fifth limitation of realignment is that the interpolation method used to estimate the new value of the fMRI signal of a voxel after the realignment is not perfect. This leads to so-called interpolation errors in the signal [9].

Realignment computes a spatial transform to generate a stabilized image of the brain. As mentioned, head movements in the scanner result in changes that a simple rigid-body transformation can not correct. For example, the head movements alter the shim of the magnet, so head motion causes changes to the intensity of some regions of the image. Andersson and colleagues have added an EPI unwarping function to SPM2 that reduces this movement-by-inhomogeneity interaction. This software compensates for the changes in image brightness that result from head movements. This unwarping stage can be selected at the same time as the realignment. This stage is computationally intensive, and typically requires more processing time than all other spatial preprocessing steps combined.

Clearly, motion creates serious consequences for fMRI data analysis. As we have discussed, a number of clever techniques have been devised to minimise motion artefacts. However, these techniques will not completely eliminate motion artefacts, in particular if the head movements are large or sudden. Therefore, if possible, head movement should be

minimized, for example, by using a head constraint. Furthermore, tasks should be designed to minimize the risk of task correlated movement.

5.2.3 Spatial normalization

During an fMRI experiment, usually, data is collected for several subjects. However, each individual.s brain differs in orientation, size and shape relative to other members in the group. Usually, the orientation, size and shape of the brains of individual subjects are changed to match the orientation, size and shape of a standard brain .There are a number of reasons why making these different brains more alike in size and shape is desirable. Firstly, when the same voxels in the brain of each subject represents the same anatomical location, comparisons between different subjects are possible .Secondly, when different brains are mapped to a certain standard brain, communication of the anatomical loci of interesting effects between different research groups becomes less arbitrary. This matching of individual brains to a standard brain is known as spatial normalization.

The orientation, size and shape of the brains of all the subjects are changed to match the orientation, size and shape of a standard brain. This standard brain is also known as a template [8].Obviously, choosing the right template is important. Optimally, the template should represent the brain of most subjects. Often, the template is based on an average of many different subjects [6].However, different scanners have unique characteristics and therefore research groups often create their own template. Even though this improves the match of the individual brain to the template for the research groups, it makes comparisons between research groups more tricky.

The matching of the orientation, size and shape of each individual to the orientation, size and shape of the template is done using 12 linear parameters; x-translation, y-translation, z-translation, roll, pitch, yaw, resizing (growing or shrinking) in three dimensions and three shear (skewing) deformations. Each of these linear parameters changes the entire brain in the same way and these are also known as affine parameters (see Figure 5.3). Note that any three points that are co-linear (a straight line can be drawn through all three points) will remain collinear after these linear transforms. In addition, each linear transform influences the entire 3D volume. As a result, linear transforms are fairly robust: small regions of signal dropout rarely have adverse influence on linear transforms as the intact portions of the image constrain the transform.

However, for the same reason, linear transforms are limited in how accurately they can match two brains: while the overall size and orientation will be matched, local features will often not be precisely aligned.

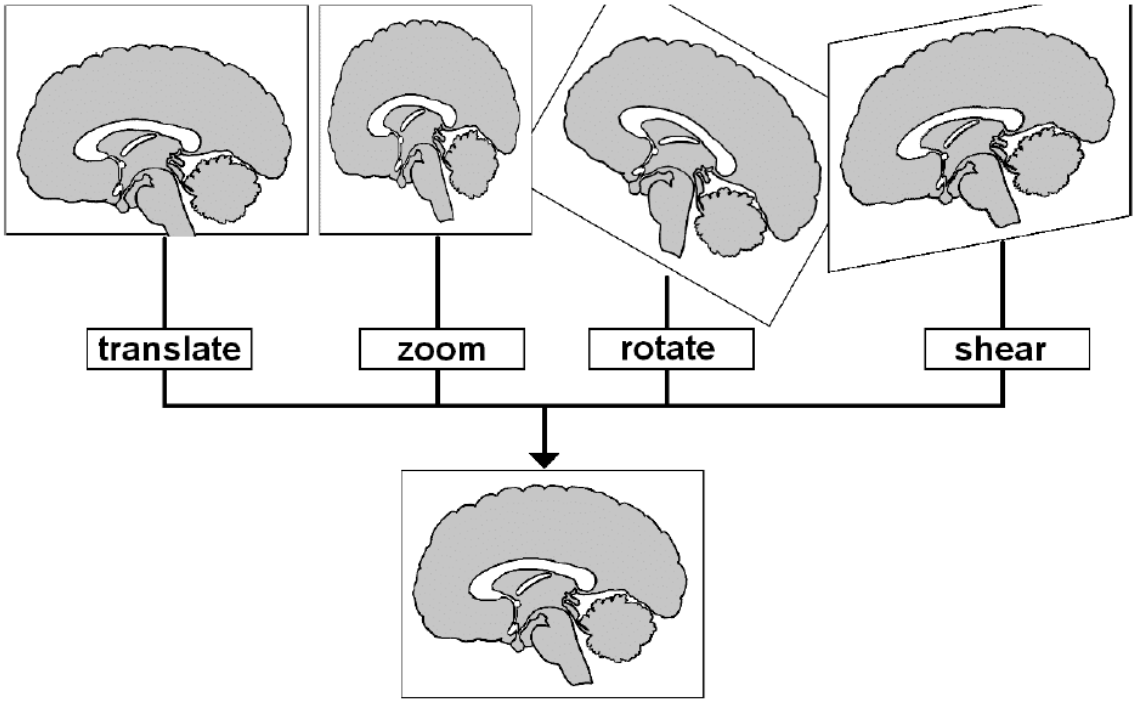

Fig 5.3: Linear transforms used for realignment (motion correction), coregistration and the first stages of normalization. The top row shows images prior to the transform, with the image at the bottom showing the result of the transform. Note that each transform can be applied in any of three dimensions (e.g. the mage can be translated in the anterior-posterior, superior-inferior or left-right dimension). Note that realignment does not typically implement or require shear transforms.

In sum, linear transforms offer a robust but rudimentary match between an individual's scan and a template image. Therefore, packages like SPM2 and AIR typically use linear transforms for the initial normalization and subsequently apply nonlinear transforms to offer a more accurate normalization. For example, SPM2 applies a set of nonlinear cosine basis functions to improve the normalization. Figure 5.4 shows how nonlinear functions can be used to aid normalization. These enable local changes in the brain, also known as warping, and potentially offer a better match to the template. A minimization algorithm for the least mean square difference between the brain volumes of the subject and the template volume is used and

the new value of the fMRI signal for a voxel after the normalization is estimated by interpolation from the values of the fMRI signal of neighbouring voxels.

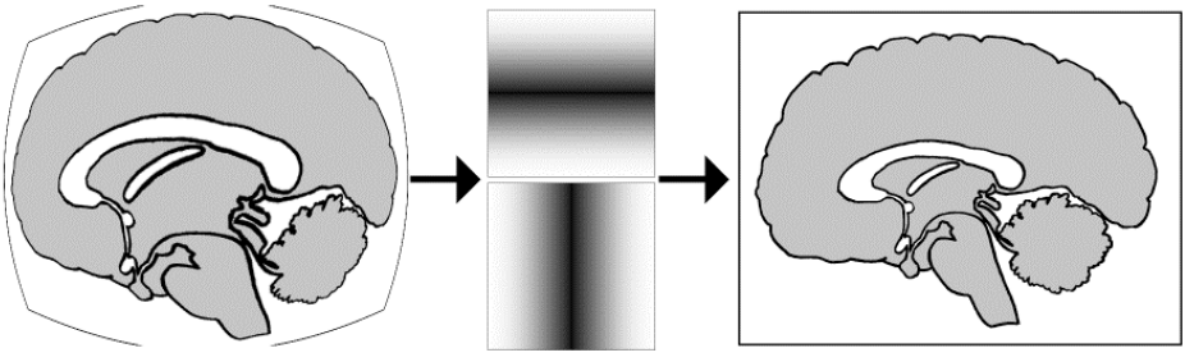

Figure 5.4: Nonlinear transforms. The image on the left cannot be made to accurately match the image on the right using only linear transforms. However, applying to nonlinear basis functions the image can be accurately normalized. These transforms are shown in the middle of the figure: one function crushes information near the vertical center of the image, while the other function crushes information near the horizontal center.

Obviously, some constraints have to be imposed on this minimization procedure, since a large difference in the amount of warping between adjacent areas can lead to unrealistic results. The constraint usually imposed is that the overall warp of the brain has to be smooth.Practically, this means minimizing the difference in the amount of warping between adjacent brain areas. The result is that normalization matches the overall orientation, size and shape of the brain of each subject to the template, but not the individual sulci. Usually, this overall matching of normalization is not considered a problem, since precise matching of each individual brain to the template would be unrealistic.

5.2.4 Spatial coregistration

In image processing terms coregistration applies to any method for aligning images.By this definition, both motion correction and normalization are forms of coregistration. However, neuroimagers tend to use the term coregistration to refer to alignment of images from different modalities. For example, matching the low resolution T2* fMRI scan to the high-resolution T1-weighted anatomical scan from the same individual.

In theory, intermodality coregistration is simpler than normalization: there should always be a perfect correspondence between different scans from the same individual (e.g. the same sulcal pattern should exist in both scans). However, note that algorithms implemented by SPM2 during motion correction and normalization assume a similar relationship between tissues in the different scans. For example, in normalization, a T1 scan will be matched to a template image with T1-contrast: with air and water (cerebral spinal fluid) appearing dark and white matter appearing bright. The difference-squared cost function will fail when this relationship is broken. For example, consider a T1 scan and a T2 scan from the same individual that are perfectly aligned with each other: the difference-squared cost function will indicate major difference between these images, as the air is dark in both images, but the water is bright in the T2 but dark in the T1 scan. In this case, the automated algorithms used by SPM.s normalization will result in images that do not accurately match each other.

Therefore, inter-modality coregistration cannot rely on a simple cost function that simply relies on the raw difference in intensity between the two images. There are two approaches that have been implemented to tackle this problem. The first technique simply normalizes each image to a corresponding template image (e.g. normalizing the T1 scan to a T1 template, and the T2* scan to a T2* template).

Next, the images are segmented into grey and white matter maps, and these resulting maps are coregistered to each other using a standard difference-squared cost function.A second technique relies on mutual information theory: this simply relies on the concept that different material will have different intensities within a scan modality (e.g. air will have a consistent brightness in the scan, and this brightness will be different from some other materials, such as white matter). This method is illustrated in Figure 5.5.

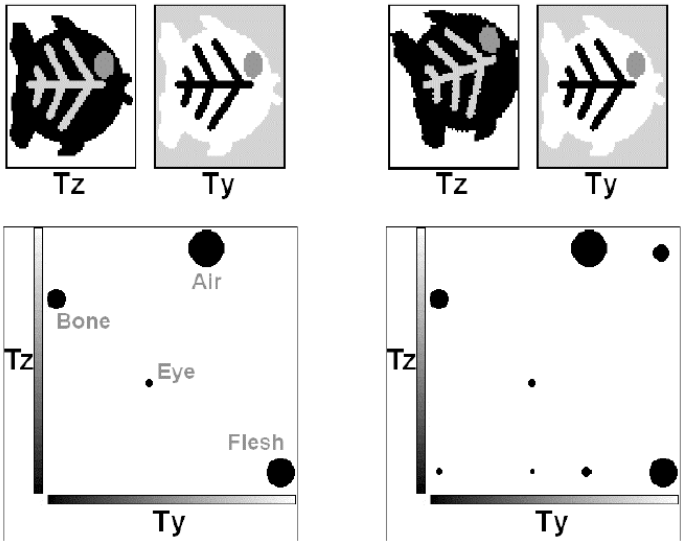

Figure 5.5: Intermodality image coregistration using mutual information theory. Consider two MRI scans using different sequences (Tz-weighted and Ty-weighted images) of the same individual. If these images are accurately aligned (top left) than the resulting image histogram will show very little noise (lower left). On the other hand, if the images are not aligned (top left), than the resulting joint histogram (lower right) will show much more noise. Therefore, we can iteratively apply linear transforms and see if they influence the entropy between the two images, eventually resulting in an accurate alignment.

5.2.5 Spatial smoothing

Spatial resolution determines how "sharp" the image looks. Spatial resolution is defined by the size of the imaging voxels. Since voxels are three dimensional rectangular solids, the resolution is frequently different in the three different directions. The size of the voxel and therefore the resolution depends on matrix size, the field-of-view (FOV), and the slice thickness. The matrix size is the number of frequency encoding steps, in one direction; and the number of phase encoding steps, in the other direction of the image plane.

An important preprocessing step is to blur the fMRI data prior to statistical analysis. At first glance, the idea of spatially smoothing data seems counterintuitive. After all, blurred data clearly degrades the spatial precision of the image. However, there are a number of important reasons for smoothing. Firstly, smoothing increases the signal to noise ratio in the fMRI signal by removing the noise present in the high spatial frequencies. In fMRI the effects of interest are produced by changes in blood flow. Changes in blood flow are expressed on a low spatial

frequency of several millimetres. Noise is usually expressed on a higher spatial frequency. Secondly, smoothing removes small frequency differences, so comparisons across subjects are made easier. Thirdly, smoothing helps to satisfy the requirements for applying Gaussian Field Theory to correct for multiple comparisons in the ensuing statistical analysis. Finally, smoothing makes the data more normally distributed [6].

Smoothing is performed by convoluting the 3D volume with a 3D Gaussian kernel. Basically this means that every data point is multiplied by a curve in the shape of a 3D normal distribution. The shape of the 3D smoothing curve should match the spatial shape of the signal, so that frequencies matching the frequencies of the 3D smoothing curve are emphasized and frequencies not matching the frequencies of the 3D smoothing curve are filtered out. The shape of the smoothing curve is defined by the Full Width Half Maximum (FWHM). This is the width of the curve at half of the maximum and is usually defined in millimetres. The FWHM chosen for the smoothing curve is typically two or three times the voxelsize. In our own work, we usually collect data with a resolution of around 3x3x3 mm, so we tend to choose an 8 mm FWHM for our smoothing filter. However, it should be noted that the smoothing acts as a spatial filter . a FWHM of 8 mm is tuned to detect clusters of around this size. Therefore, if you have an a priori prediction of the size of the region you hope to measure, you can set your smoothing filter to maximize signals for that size of region (for example, if you wanted to examine the tiny superior colliculi you would want to select a smaller smoothing filter than if you were interested in a larger region such as early visual cortex). The end result of this spatial smoothing is therefore that high spatial frequencies in the signal are filtered out while low spatial frequencies in the signal are emphasized [6].

5.2.6 Physiological Noise Correction

The magnetic field in the head changes during breathing because of the bulk motion of the thorax. Breathing patterns may change the fMRI signal more than the desirable BOLD response. Changes in the respiratory rhythm and volume can also change the CO_2 level in the blood and cause BOLD signal fluctuations. The pulse is also known to cause artifacts. Techniques have been developed to remove cardiorespiratory artifacts during offline analysis, but they have not been adapted to online processing for real-time fMRI. Recently van Gembris

[10] reported a real-time shimming method to compensate for respiration induced fluctuations in the main magnetic field (B0 field). Future implementations of fMRI-BCI could potentially explore the use of these methods for correction of physiological artifacts and noise. This becomes even more important at higher static magnetic fields, because the relative contribution of physiology to the noise increases.

5.3 Statistical analysis

While the majority of work in fMRI has used conventional neuorimaging methods of univariate analysis, there is a growing interest in incorporating multivariate methods of pattern analysis using machine learning techniques in the emerging field of brain state detection. In this section, we will consider both methods as applied to fMRI.

5.3.1 UNIVARIATE ANALYSIS

Univariate methods seek to find out how a particular perceptual or cognitive state is encoded by measuring brain activity from many thousands of locations repeatedly but then analyzing each location separately. If the responses at any brain location differ between two states, then it is possible to use measurements of the activity at that location to determine or decode the state. A commonly used method for detecting neuronal activity from fMRI time series is correlation analysis. The method computes correlation coefficients between the time-series of the reference vector representing the expected hemodynamic response and the measurement vector of each voxel. A primary advantage of this method is that the reference vector can have an arbitrary shape best reflecting the hemodynamic response. Gembris [10] presented a computationally efficient algorithm, implemented in the analysis software Functional Magnetic Resonance Imaging in Real-time (FIRE), which generates correlation coefficients on a "sliding-window" of the fMRI time series. The basic concept of this method is to restrict the correlation computation to only the most recent data sets. According to this method, definition of the correlation coefficient in combination with detrending is given by the equation:

$$\rho = \frac{\vec{x}\,\vec{rs}}{\left\|\vec{x}\right\|\left\|\vec{rs}\right\|} \qquad \text{..... (5.1)}$$

where $\vec{x}$ is the measurement vector of one voxel that is updated at every time step, $\vec{rs}$ is the reference vector, and $\vec{x}$ and $\vec{rs}$ are detrending vectors. Each new data set replaces the data set of the previously acquired sliding-window buffer. This method reduces the load on memory and computational time, two important factors that critically affect the performance of fMRI-BCI. The authors tested the method in an experiment with 20 healthy participants in a paradigm comprising alternating baseline and visual stimulation blocks. The sliding window correlation method successfully identified the visual areas as being significantly active with voxels in this region crossing the threshold correlation coefficient of 70%. The method offers greater sensitivity of the correlation coefficients to changes in the signal response shape and amplitude with passing measurements. Another advantage of the sliding window technique is its capability for quantifying physiological variability when combined with a technique called reference vector optimization. This method takes into account a realistic model of the hemodynamic response function to adapt the reference vector to the measured data and thus increases functional sensitivity.

The General Lineal Model (GLM) provides by far the most unified framework in the analysis of the fMRI data. GLM can model multiple experimental and confounding effects simultaneously. Bagarinao et al. presented a method for real-time estimation of GLM coefficients. The observed fMRI data are considered a linear combination of L explanatory functions $f_i(.)$ and an error term:

$$y_{k,s} = b_{k,1} f_1(t_s) + \cdots + b_{k,1} f_L(t_s) + \varepsilon_{k,s} \qquad \text{.....(5.2)}$$

where $y_{k,s}$ is the observation of k^{th} voxel at time t_s, $s = 1 \ldots n$ are scan numbers, $f_s(.)$ are basis functions that span the fMRI responses for a given experiment, b_k are coefficients that need to be estimated and $\varepsilon_{k,s}$ is the residual error or noise term. The method converts the basis functions or explanatory variables of a GLM into orthogonal functions using an algorithm called the Gram-Schmidt orthogonalization procedure. The coefficients of the orthogonal functions are then estimated using the orthogonality condition.

In a conventional GLM analysis of fMRI data, multiple trials are required to identify significantly activated voxels with sufficient consistency. However, it is not possible to obtain many trials in an fMRI-BCI setting with its very need for identifying significantly active voxels in real-time. The advantage of the real-time GLM implementation is that estimates can be updated when new image data are available, making the approach suitable for fMRI-BCIs. Furthermore, with this approach it is not necessary to store the data as the data are immediately used in computing the estimates, thus reducing the memory requirements. A similar approach is taken by the analysis software (TBV) running on our local fMRI-BCI setup at the University of Tübingen, which uses the recursive least squares regression algorithm to incrementally update the GLM estimates.

After identification of the significantly active voxels, either by the method of real-time correlation or GLM analysis, their values are passed to the signal feedback subsystem at every time point for computation and presentation of the feedback to the participant.

5.3.2 MULTIVARIATE ANALYSIS

Using univariate analysis it is often difficult to find individual locations where the differences between conditions are large enough to allow for efficient decoding. In contrast to the conventional analysis, recent work shows that the sensitivity of human neuroimaging may be improved by taking into account the spatial pattern of brain activity. Pattern-based methods use considerably more information for detecting the current state from measurements of brain activity. In the previous studies with fMRI-BCI, brain signals from only one or two ROIs were extracted for providing neurofeedback to the subject. A major argument for moving away from deriving feedback signals from single ROIs is that perceptual, cognitive, or emotional activities generally recruit a distributed network of brain regions rather than single locations. Pattern-based methods not only use voxel-intensities but also their spatiotemporal relationships.

Several studies have previously reported offline classification of fMRI signals using various pattern-based methods such as multilayer neural networks, Fisher Linear Discriminant (FLD) classifier[11], and support vector machines (SVMs). Laconte et al. [11]. recently reported probably the first implementation of a real-time pattern classification system that could be applied to neurofeedback and BCI. The aim of the study was to first train a classification model

based on early fMRI data and thereafter to use the classifier to predict the brain state with each acquired image and alter the stimulus based on the estimated brain state. The modified Siemens scanner's image calculation environment (ICE) can be used to perform SVM classification during training and testing and then transmitted the classification results to a stimulus display computer. To improve the efficiency of classification the authors implemented a method for segmenting brain regions from nonbrain regions with a combination of intensity thresholded mask and an additional variance mask to remove signals from the eye regions. For SVM classification, images from each scan were represented as a vector whose components were intensity values for each brain voxel at that time. The experimental condition associated with each vector was represented as a scalar class label. The SVM algorithm attempts to find a decision boundary as a separating hyperplane to discriminate between the two class labels. Once the SVM model was determined from the training images, independent testing images were classified into the specified labels. Percentage classification accuracy was reported as the ratio of number of correctly classified scans to the total number of scans. To test this approach the authors used an experimental task consisting of rapid button press blocks that alternatively used the left or right portion of the visual display. During the training runs an arrow in the center of the display pointed toward the left or right target acted as the cue. During the subsequent testing run, each acquired image was classified by the SVM model, and the arrow was updated in terms of its position and orientation based on the classifier's left or right decision. With additional subjects, task instructions were changed to further examine pattern classification of mood, language, and imagined motor tasks. The authors concluded that real-time pattern classification of brain states using fMRI data is possible; high prediction accuracies are attainable during sustained activation; and stimulus feedback based on pattern classification can respond to changes in brain states much earlier than the time to- peak limitations of the BOLD response. The above approach is limited to two-class classification of brain states.

We have recently implemented in our fMRI-BCI a multiclass pattern classification system that offers the experimenter the flexibility of selecting either an SVM or a multilayer neural network classification algorithm [11]. Mourao-Miranda et al.[11] carried out a comparison of two methods, SVM and Fisher Linear Discriminant classifier (FLD), for classifying multisubject data from an experiment involving a face matching and location matching task. They demonstrated that SVM outperforms FLD in classification accuracy as well

as in the robustness of the spatial maps obtained. Further work needs to be carried out to rigorously compare the performance of existing pattern classification approaches to assess their suitability and efficacy for fMRI brain state classification.

CHAPTER 6

OUR WORK

The most important advantage of MR imaging is that it is a non-invasive technique. The use of computer technology in medical decision support is now widespread and pervasive across a wide range of medical area, such as cancer research, gastroenterology, heart diseases, brain tumors, etc. Fully automatic normal and diseased human brain classification can be obtained from magnetic resonance images; which is a great importance for research and clinical studies.

Recent work [12,14] has shown that classification of human brain in magnetic resonance (MR) images is possible via supervised techniques such as artificial neural networks and support vector machine (SVM) , and unsupervised classification techniques such as self-organization map (SOM) and fuzzy c -means [14]. Other supervised classification techniques, such as k -nearest neighbors (k -NN) can be used to classify the normal/pathological T2-weighted MRI images. In this study, we used supervised machine learning algorithms (ANN and k -NN) to obtain the classification of images under two categories, either normal or abnormal.

Wavelet transform is an effective tool for feature extraction, because they allow analysis of images at various levels of resolution. This technique requires large storage and is computationally more expensive [13]. Hence an alternative method for dimension reduction scheme is used. In order to reduce the feature vector dimension and increase the discriminative power, the principal component analysis (PCA) has been used. Principal component analysis is appealing since it effectively reduces the dimensionality of the data and therefore reduces the computational cost of analyzing new data. To perform the classification on the input data, the SVM have been used.

The contribution of our work is the integration of an efficient feature extraction tool and a robust classifier to perform a more robust and accurate automated MRI normal/abnormal brain images classification. Also, this paper focuses on a comparison of our results with a similar study using supervised and unsupervised methods that were carried out by other authors [12,14].

In our work first, features are extracted using wavelet transformation. Wavelets seem to be a suitable tool for this task, because they allow analysis of images at various levels of

resolution [12]. second, principal component analysis (PCA) is used for reducing the number of features and also increasing discrimination between classes. Principal component analysis is appealing since it effectively reduces the dimensionality of the data and therefore reduces the computational cost of analyzing new data. Finally, the pattern recognition methods SVM are used for classification. The results indicate fully classification of data. Our work is the extension and modification of the method introduced in [12]. But, our case is different, the database contains more and different images, we use pre-processing step and additional classifier; the number of features obtained by PCA for maximum classification rate is less and we obtain better classification rate.

6.1 Wavelet Transform

A wavelet is a "small wave" of varying frequency and limited duration. Using narrow windows for analyzing high frequencies and wide windows for analyzing low frequencies works quite well for signals having high frequency components for short durations and low frequency components for long durations.

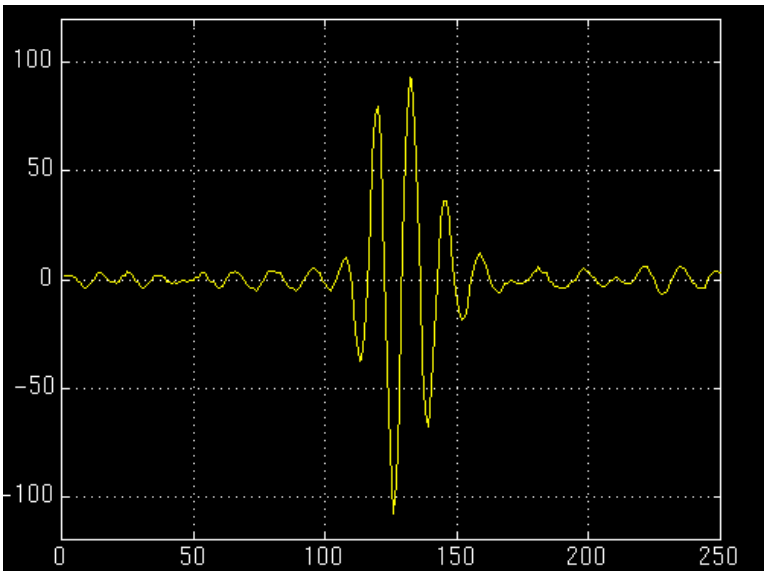

Fig. 6.1 Wavelet Function

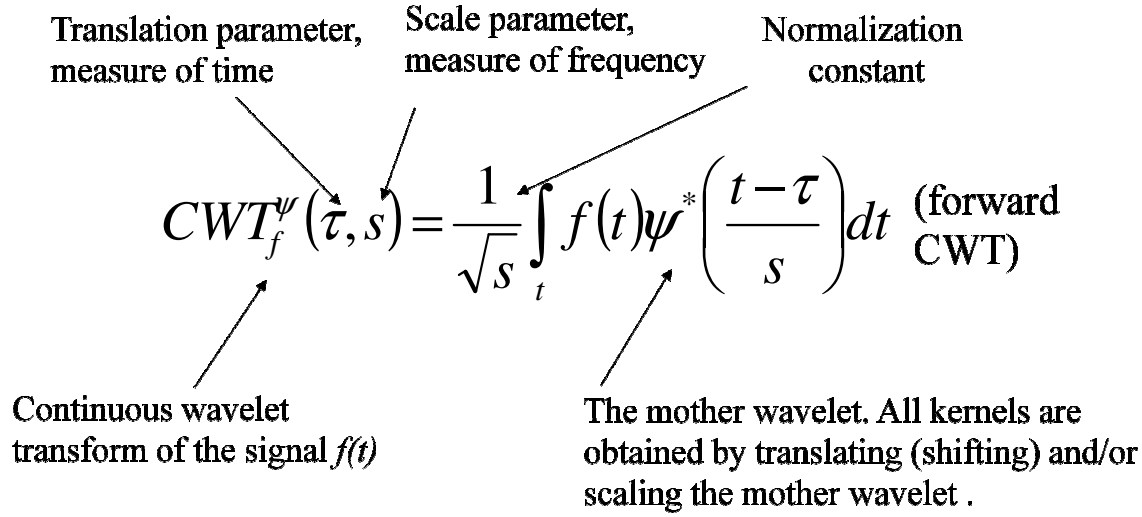

Scale = 1/frequency

Wavelets provide simultaneous localization in time and scale (i.e, frequency).The location of the wavelet allows to explicitly represent the location of events in time. The shape of the wavelet allows to represent different detail or resolution.

6.1.1 Discrete Wavelet Transform

The DWT is an implementation of the wavelet transform using a discrete set of the wavelet scales and translation obeying some defined rules. For practical computations, it is necessary to discretize the wavelet transform. The scale parameter(s) is (are) discretized on alogarithmic grid. The translation parameter (t) is then discretized with respect to the scale parameter, i.e. sampling is done on the dyadic (as the base of the logarithm is usually chosen as two) sampling grid. The discretized scale and translation parameters are given by, $s = 2^{-m}$ and $t = n\, 2^{-m}$,where m, n ϵ Z , the set of all integers. Thus, the family of wavelet functions is represented in

$$\psi_{jk}(t) = \sqrt{2^{-j}}\,\psi\left(2^{-j}t - k\right) \quad j,k \in Z \qquad \text{..... (6.1)}$$

Forward DWT:

$$a_{jk} = \sum_t f(t)\,\psi^*_{jk}(t) \qquad \text{..... (6.2)}$$

Inverse DWT:

$$f(t)=\sum_{k}\sum_{j}a_{jk}\psi_{jk}(t) \qquad \ldots\ldots\ldots\ldots\ldots\ldots (6.3)$$

6.1.2 Regularity and Wavelet Vanishing Moments

Wavelet transform of a function *f(x)* provide information about special feature of *f(x)*. Lipschitz regularity of a function *f(x)* in an interval tells about highest order derivative of function *f(x)* that can exist in that interval. If a function *f(x)* has highest order derivative 'm' then this feature of *f(x)* can be detected by a wavelet function ψ(x) having 'm' vanishing moments. Wavelet function ψ(t) having 'm' vanishing moments is given by

$$\psi(t)=(-1)^{m}\frac{d^{m}\phi(t)}{dt^{m}} \qquad \ldots\ldots\ldots\ldots\ldots\ldots (6.4)$$

For higher scales

$$Wf(u,s)=s^{m}f*\frac{d^{m}\overline{\phi_{s}}}{dt^{m}}(s)=s^{m}\frac{d^{m}}{du^{m}}\left(f*\overline{\phi_{s}}\right)(s) \qquad \ldots\ldots\ldots\ldots\ldots\ldots (6.5)$$

Wavelet transform of a function f*(x)* with wavelet function ψ(t) having 'm' vanishing moments will have maximum value at points where m^{th} derivative of *f(x)* will be maximum. At these points derivative of wavelet transform will nullify or have a singularity. Derivative of wavelet transform with wavelet function ψ(t) having 'm' vanishing moments is equivalent to wavelet transform with wavelet function ψ'(t) having 'm+1' vanishing moments. Number of maxima at a given scale increase linearly with number of moments in wavelet. Fourier transform ψ(ω) of ψ(t) having 'm' vanishing moments and it's first 'm-1' derivatives are zero at ω=0

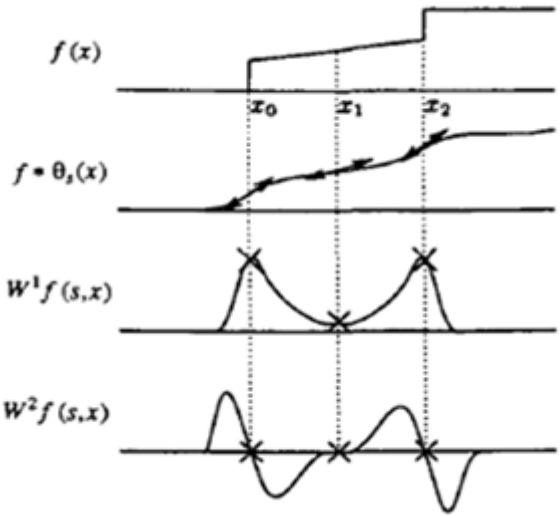

Fig 6.2 Extrema of $W^1 f(s,x)$ and the zero crossing of $W^2 f(s,x)$ are the inflection points of $f*\theta_5(x)$. Points of abscissa x_0 and x_2 are sharp variations of $f*\theta_5(x)$ and are local maxima of $\left|W^1 f(s,x)\right|$. The local minimum of $\left|W^1 f(s,x)\right|$ at x_1 is also an inflection point but it is a slow variation point.

In order to minimize the amount of computations, we should have the minimum number of maxima necessary to detect the interesting irregular behavior of the signal. This means that we must choose a wavelet with as few vanishing moments as possible, but with enough moments to detect the Lipschitz exponents of highest order that we are interested in. A wavelet with *n* vanishing moments has at least *n + 1 local extrema. For* numerical computations, it is better to choose a wavelet with exactly *n + 1 local extrema.*

In image processing, we often want to detect discontinuities and peaks that have Lipschitz exponents smaller than one [15]. It is, therefore, sufficient to use a wavelet with only one vanishing moment. In signals obtained from turbulent fluids, interesting structures have a Lipschitz exponent between 0 and 2 . We, thus, need a wavelet with two vanishing moments to analyze turbulent structures.

Singularity are the points where wavelet transform is maximum. Wavelet transform is maximum when it get a feature for which it is created for example in image processing wavelet function used for edge detection has only one vanishing moment therefore wavelet transform formed using this wavelet function will have maximum value at edges. But this type of edge detection increase with scaling factor.

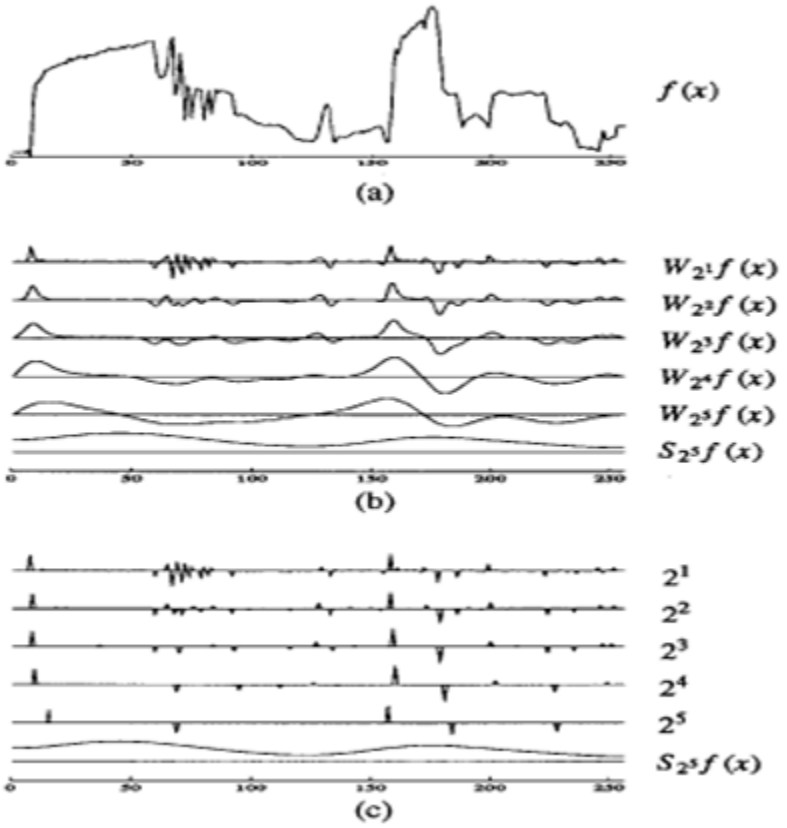

Fig 6.3 (a): Image scan line of 256 samples. (b): Dyadic wavelet transform of signal 1(a), on 5 scale (2^5), we keep the remaining low-frequencies $S_2{}^5 f(x)$ to have the complete representation. (c): Maxima representation of wavelet transform shown in (b). Each dirac indicate the position and amplitude of local maxima at the corresponding scale of Dyadic wavelet transform.

$$f(t) = \sum_k c_k \varphi(t-k) + \sum_k \sum_j d_{jk} \psi(2^j t - k) \quad \ldots\ldots\ldots\ldots\ldots\ldots (6.6)$$

V_0 — basis functions

$W_0, W_1, W_2, \ldots$ — wavelet functions

6.1.3 Multi-resolution using Wavelet Transform:

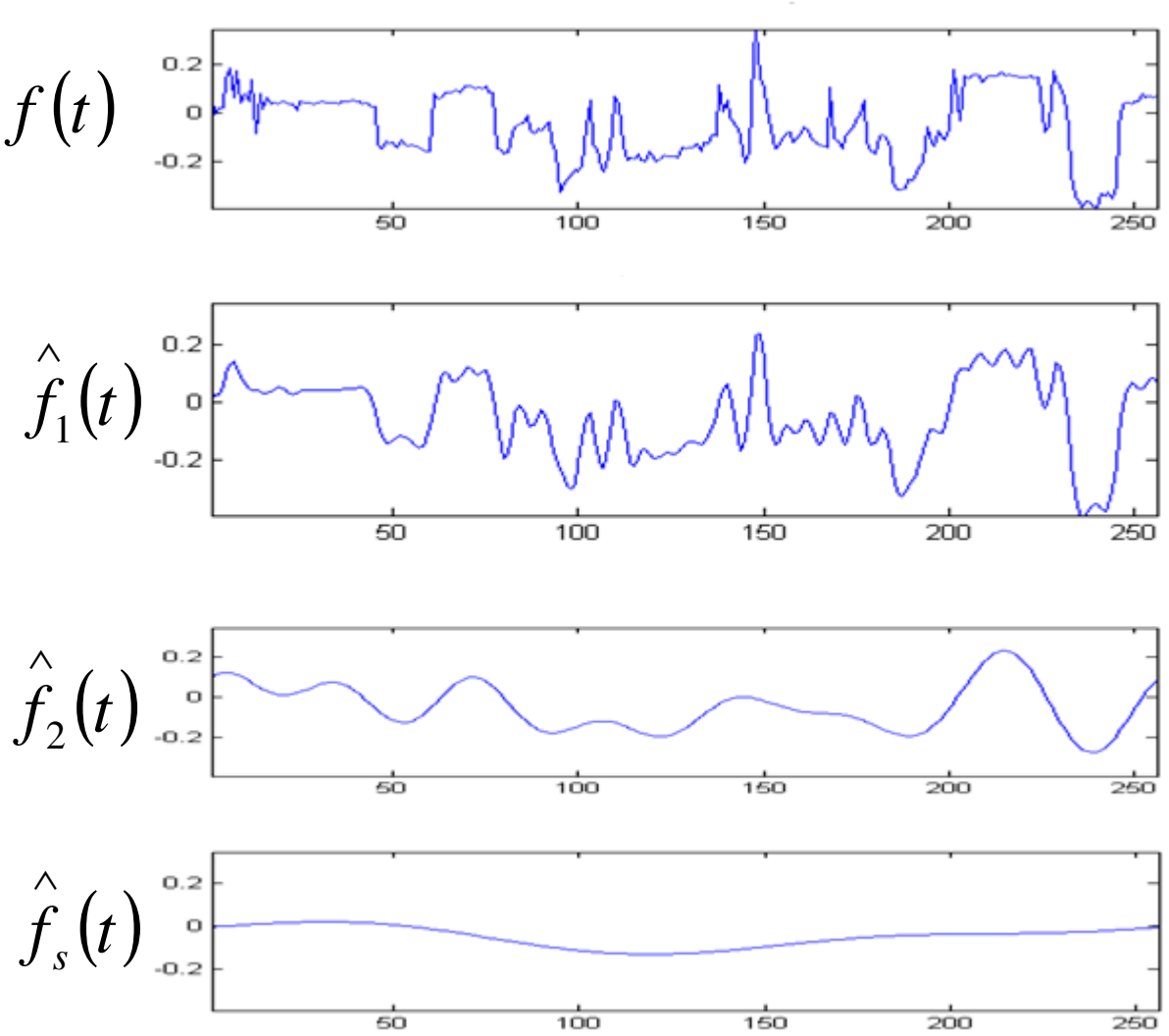

If a set of functions can be represented by a weighted sum of ψ(*t* - *k*), then a larger set (including the original) can be represented by a weighted sum of ψ(2*t* - *k*).

Basis functions:

V_j : space spanned by $\psi(2^j t - k)$

f(t) ϵ V_j $f(t) = \sum_k \sum_j a_{jk} \psi_{jk}(t)$ ..... (6.7)

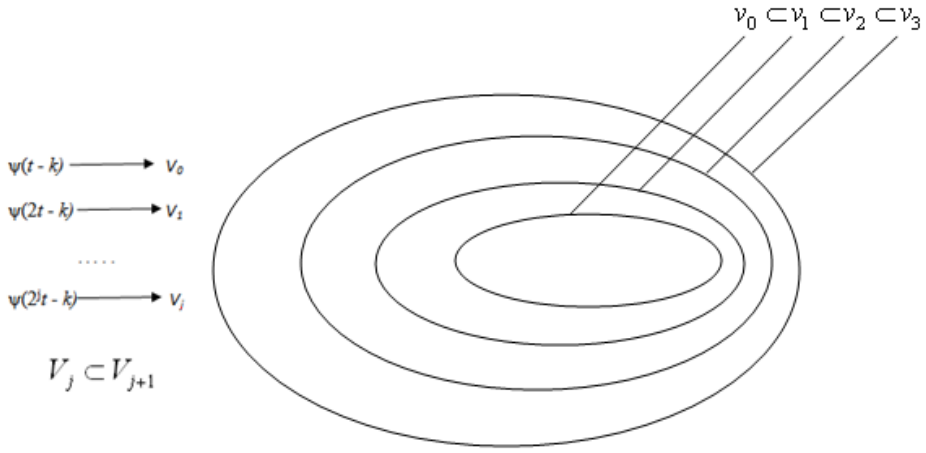

Fig. 6.4 Multiresolution conditions → nested spanned spaces: $V_j \subset V_{j+1}$ i.e., if f(t) ϵ V_j then f(t) ϵ V_{j+1}

Let W_j be the orthogonal complement of V_j in V_{j+1} i.e., all functions in V_{j+1} that are orthogonal to all functions in V_j.

$$V_{j+1} = V_j + W_j \qquad \text{..... (6.8)}$$

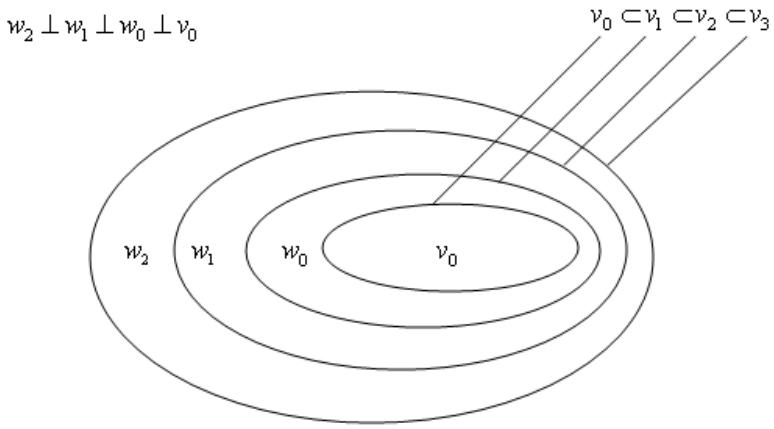

Fig. 6.5 All functions in V_{j+1} that are orthogonal to all functions in V_j.

If f(t) ϵ V_{j+1}, then f(t) can be represented using basis functions from V_{j+1}:

$$f(t) = \sum_k c_k \varphi\left(2^{j+1}t - k\right) \leftarrow V_{j+1} \quad \text{..... (6.9)}$$

Alternatively, f(t) can be represented using basis functions from V_j and W_j:

$$V_{j+1} = V_j + W_j$$

$$f(t) = \sum_k c_k \varphi\left(2^j t - k\right) + \sum_k \sum_j d_{jk} \psi\left(2^j t - k\right) \quad \text{..... (6.10)}$$

(φ term: V_j; ψ term: W_j)

$V_{j+1} = V_j + W_j$ using recursion on V_j :

$$V_{j+1} = V_{j-1} + W_{j-1} + W_j = \ldots = V_0 + W_0 + W_1 + W_2 + \ldots + W_j$$

..... (6.11)

$$f(t) = \sum_k c_k \varphi(t - k) + \sum_k \sum_j d_{jk} \psi\left(2^j t - k\right)$$

(φ term: V_0; ψ term: $W_0, W_1, W_2, \ldots$)

Example: Suppose we are given a 1D "image" with a resolution of 4 pixels:[9 7 3 5]

This image can be represented in the Haar basis as follows:

- Start by averaging the pixels together (pairwise) to get a new lower resolution image:

[8 4] (averaged and subsampled)

- To recover the original four pixels from the two averaged pixels, store some *detail coefficients.*

Resolution	*Averages*	*Detail Coefficients*
4	[9 7 3 5]	[]
2	[8 4]	[1 −1]

- Repeating this process on the averages gives the full decomposition:

Resolution	*Averages*	*Detail Coefficients*
4	[9 7 3 5]	[]
2	[8 4]	[1 −1]
1	[6]	[2]

- The Harr decomposition of the original four-pixel image is:

$$[6 \;\; 2 \;\; 1 \;\; -1]$$

- We can reconstruct the original image to a resolution by adding or subtracting the detail coefficients from the lower-resolution versions.

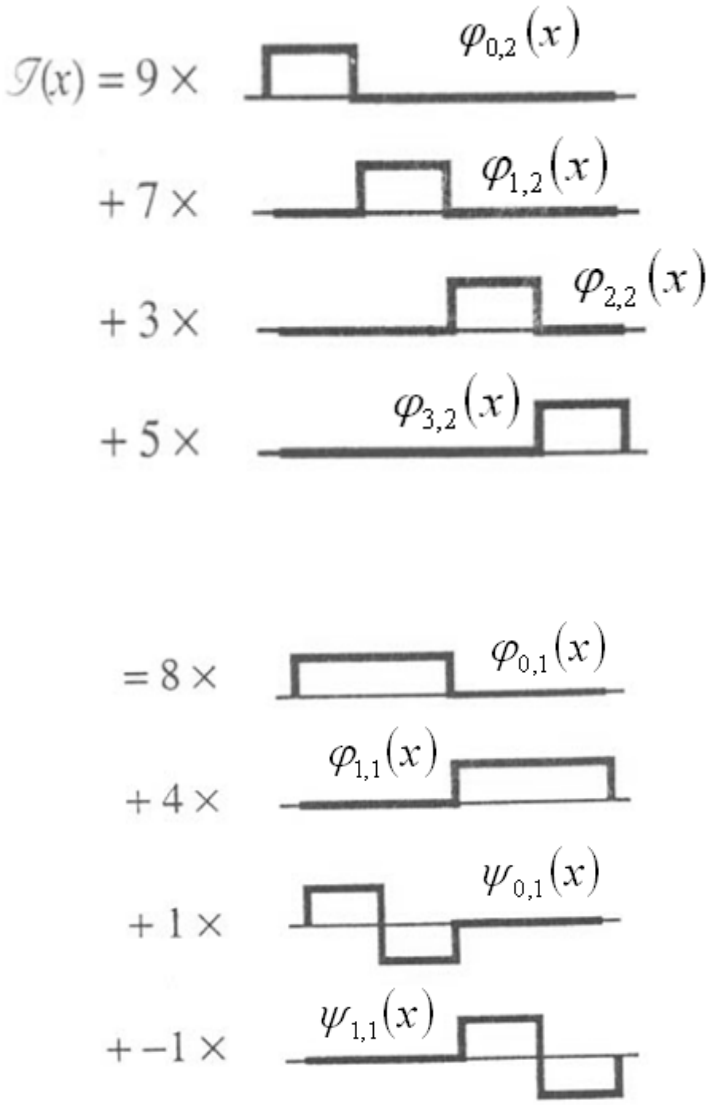

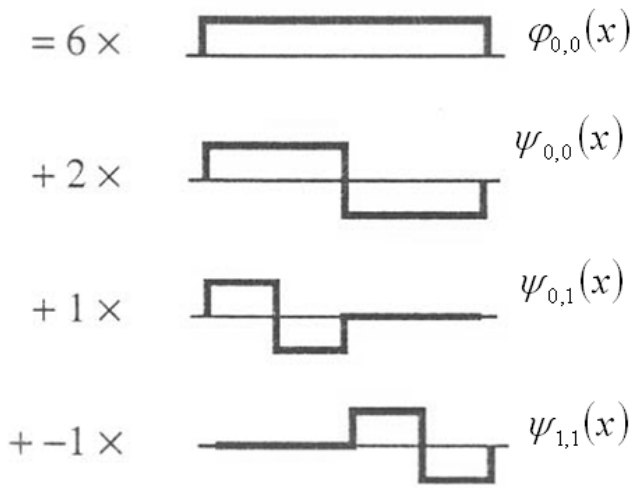

6.1.4 Two Dimensional Wavelet Transform:

Scaling function:

$$\varphi(x, y) = \varphi(x)\varphi(y) \qquad \text{…… (6.12.1)}$$

Wavelet functions:

$$\psi^H(x, y) = \psi(x)\varphi(y) \quad \text{Horizontal direction} \qquad \text{…… (6.12.2)}$$

$$\psi^V(x, y) = \varphi(x)\psi(y) \quad \text{Vertical direction} \qquad \text{…….. (6.12.3)}$$

$$\psi^D(x, y) = \psi(x)\psi(y) \quad \text{Diagonal direction} \qquad \text{…… (6.12.4)}$$

Wavelet Toolbox in matlab: Write “wavemenu” in matlab command window to use matlab tool box

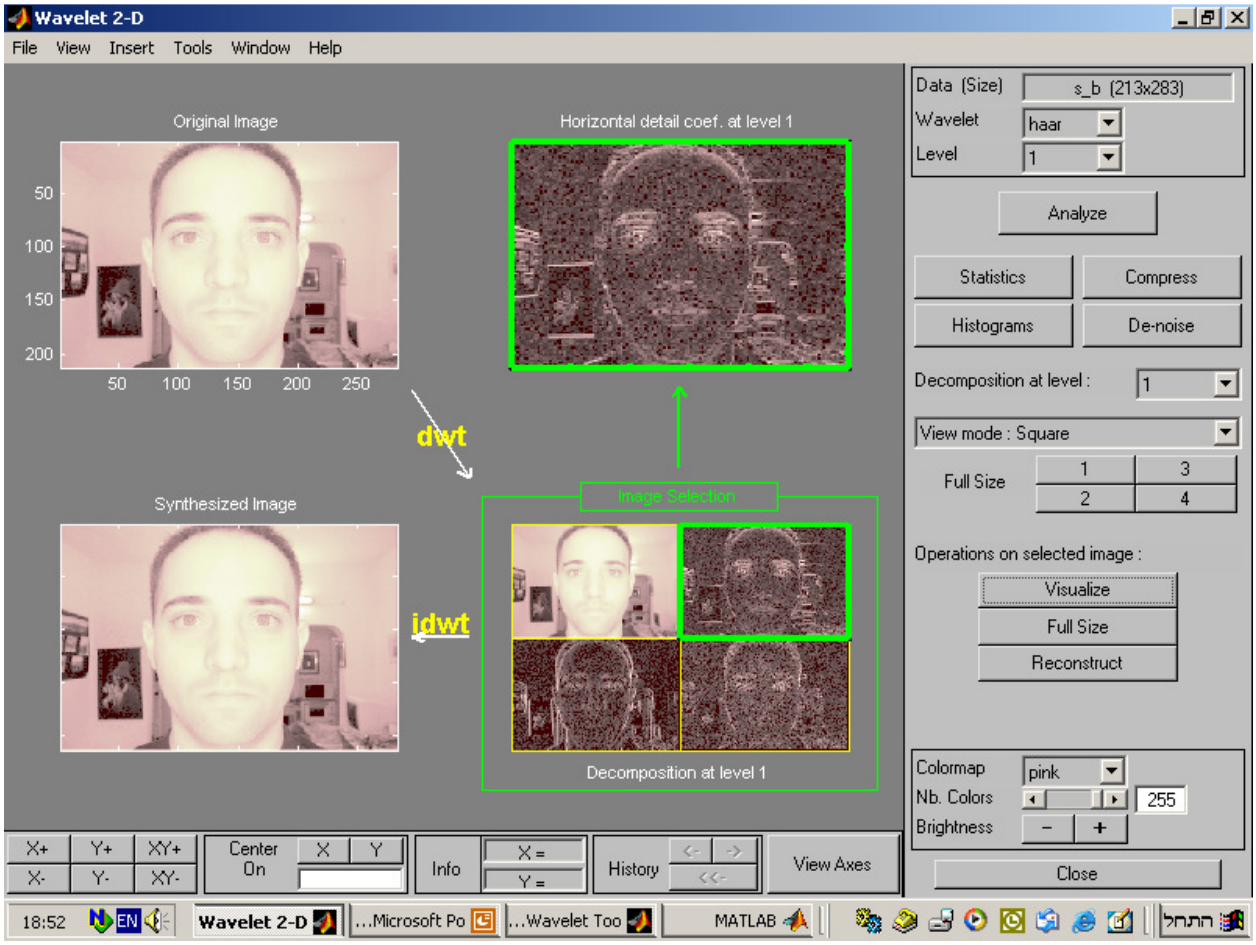

Fig. 6.6 Wavelet Toolbox in Matlab

6.1.5 Feature Extraction Using Wavelet Transform

In discussion it is clear how a lower resolution image is obtained using wavelet transform. In our work we have done two level wavelet decomposition and image of lower resolution is taken for feature extraction purpose.

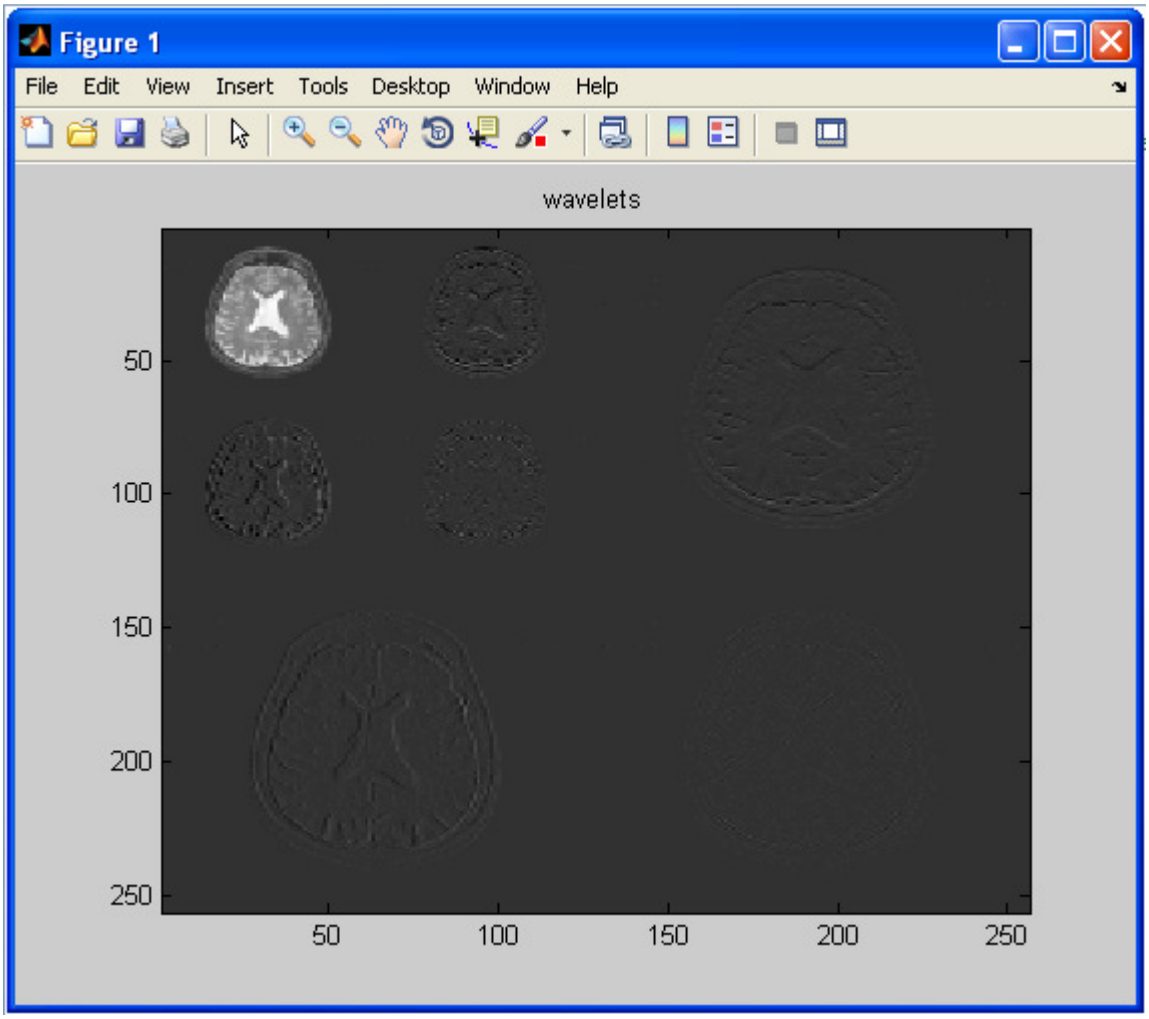

Fig 6.7 Wavelet decomposition for feature extraction

6.2 Principal Component Analysis

After taking lower resolution image from wavelet decomposition for feature extraction we apply feature reduction techniques. The principal component analysis and independent component analysis (ICA) are two well-known tools for transforming the existing input features into a new lower-dimension feature space. In PCA, the input feature space is transformed into a lower-dimensional feature space using the largest eigenvectors of the correlation matrix. In the ICA, the original input space is transformed into an independent feature space with a dimension that is independent of the other dimensions. PCA is the most widely used subspace projection technique. These methods provide suboptimal solution with a low computational cost and computational complexity.

Implementing PCA in image processing: Let we have a database of M images each of size N×N.

Step 1: Image I is converted to a vector Γ of size $N^2 \times 1$.

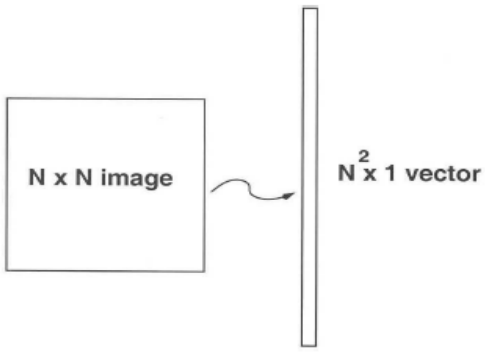

Each image is converted to a vector Γ_i of size $N^2 \times 1$.

Step 2:Compute average face vector Ψ.

$$\psi = \frac{1}{M}\sum_{i=1}^{M}\Gamma_i \qquad \ldots\ldots\ldots\ldots\ldots\ldots (6.13)$$

Step 3:Subtract the mean Face

$$\phi_i = \Gamma_i - \psi \qquad \ldots\ldots\ldots\ldots\ldots\ldots (6.14)$$

Step 4:Compute the covariance Matrix C:

$$C = \frac{1}{M}\sum_{i=1}^{M}\phi_i\phi_i^T = AA^T \qquad \left(N^2 \times N^2\ Matrix\right)$$

$$where\ A = \left[\phi_1 \quad \phi_2 \quad .... \quad \phi_M\right] \quad \left(N^2 \times M\ Matrix\right) \qquad \text{..... (6.15)}$$

Step 5:Compute the eigen vectors u_i of AA^T:

Matrix AA^T is very large not practical

Step 5.1: Consider matrix A^TA (M×M Matrix)

Step 5.2: Compute the eigen vectors v_i of A^TA (M×M Matrix)

$$A^TAv_i = \mu_i v_i \qquad \text{..... (6.16)}$$

Relation between u_i and v_i

$$A^TAv_i = \mu_i v_i \Rightarrow AA^TAv_i = \mu_i Av_i \Rightarrow$$

$$CAv_i = \mu_i Av_i \Rightarrow Cu_i = \mu_i u_i \quad where \quad u_i = Av_i$$

..... (6.17)

Thus AA^T and A^TA have same eigen values and their eigen vectors are related as $u_i = Av_i$

Note 1: AA^T can have up to N^2 eigen values and eigen vectors.

Note 2: A^TA can have up to M eigen values and eigen vectors.

Note3: M eigen values of A^TA (along with their corresponding eigen vectors) correspond to M largest eigen values of AA^T(along with their corresponding eigen vectors).

Step 5.3: Compute best eigen vectors of AA^T : $u_i = Av_i$

Important: Normalize u_i such that $\|u_i\| = 1$

Step 5: Keep only K eigen vectors (corresponding to K largest eigen values).

Example:

- Each face (minus the mean) Φ_i in the training set can be represented as a linear combination of the best K eigenvectors:

$$\hat{\Phi}_i - mean = \sum_{j=1}^{K} w_j u_j, \quad (w_j = u_j^T \Phi_i)$$

(we call the u_j's *eigenfaces*)

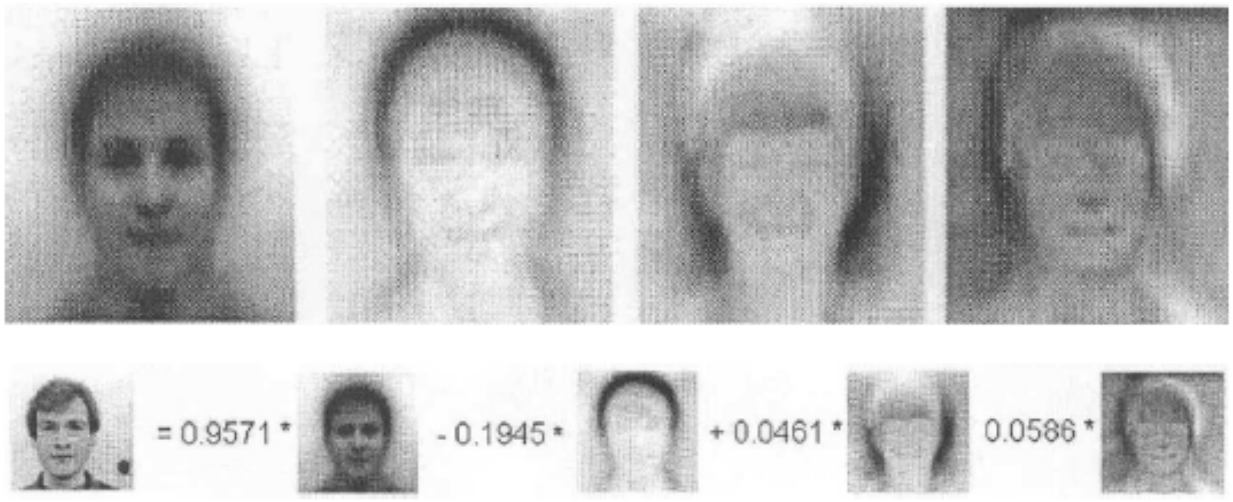

Fig. 6.8 Principal component decomposition of Face

6.3 Support Vector Machine

In feature reduction procedure we decompose each image in seven major components (along significant eigen vectors).Weights of each image along these eigen vectors will be used for classification purpose. For classification we use support vector machine as a classifier.

SVM is a binary classification method that takes as input labeled data from two classes and outputs a model file for classifying new unlabeled/ labeled data into one of two classes . The SVM originated from the idea of the structural risk minimization that was developed by Vapnik. Support vector machines are primarily two class classifiers that have been shown to be attractive and more systematic to learning linear or non-linear class boundaries. The use of SVM, like any other machine learning technique, involves two basic steps namely training and testing. Training

an SVM involves feeding known data to the SVM along with previously known decision values, thus forming a finite training set. It is from the training set that an SVM gets its intelligence to classify unknown data.

The key concept of SVM is the use of hyperplanes to define decision boundaries separating between data points of different classes. SVMs are able to handle both simple, linear, classification tasks, as well as more complex, i.e. nonlinear, classification problems. Both separable and nonseparable problems are handled by SVMs in the linear and nonlinear case. The idea behind SVMs is to map the original data points from the input space to a high-dimensional, or even infinite-dimensional, feature space such that the classification problem becomes simpler in the feature space. The mapping is done by a suitable choice of a kernel function.

Consider a training data set $\{(x_i, y_i)\}_{i=1}^{N}$ with $x_i \in R^d$ x_i being the input vectors and $y_i \in \{-1,+1\}$ the class labels. SVMs map the d- dimensional input vector x from the input space to the d_h dimensional feature space using a (non) linear function $\varphi(.):R^d \rightarrow R^d_h$. The separating hyperplane in the feature space is then defined as $w^T\phi(x)+b=0$ with b ϵ R and w an unknown vector with same dimension as φ(x). A data point x is assigned to the first class if $f(x)=sign(w^T\phi(x)+b)$ equal to +1 or to the second class if *f(x)* equals -1.

In case the data are linearly separable, the separating hyperplane can be defined in many ways. However, SVMs are based on the maximum margin principle, and aim at constructing a hyperplane with maximal distance between the two classes. The SVM classifier starts from the following formulations

$$w^T\phi(x)+b \geq +1 \quad for \quad y_i = +1$$

$$w^T\phi(x)+b \leq -1 \quad for \quad y_i = -1$$

Equivalent to

$$y_i\left(w^T\phi(x)+b\right) \geq +1 \qquad i = 1,.....,N \qquad \text{..... (6.18)}$$

The classifier is written as

$$f(x) = sign\left(w^T \phi(x) + b\right)$$

In Figure 6.8, SVM classification with a hyper plane that minimizes the separating margin between the two classes are indicated by data points marked by "X" s and "O"s. Support vectors are elements of the training set that lie on the boundary hyper planes of the two classes.

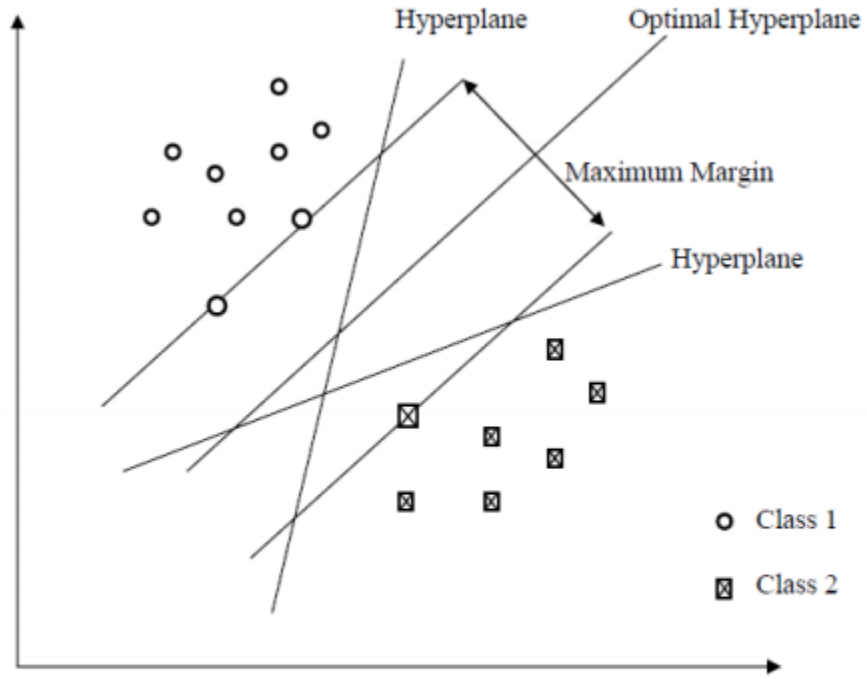

Fig.6.9 Illustration of a separating hyperplane (solid line) with a maximal margin determined by a linear SVM. (Selvaraj *et. al*, 2007).

6.4 Simulation and Results

The MRI data is collected from the Harvard Medical School website [16] http:// med.harvard.edu/AANLIB/

Training Data

Class 1:

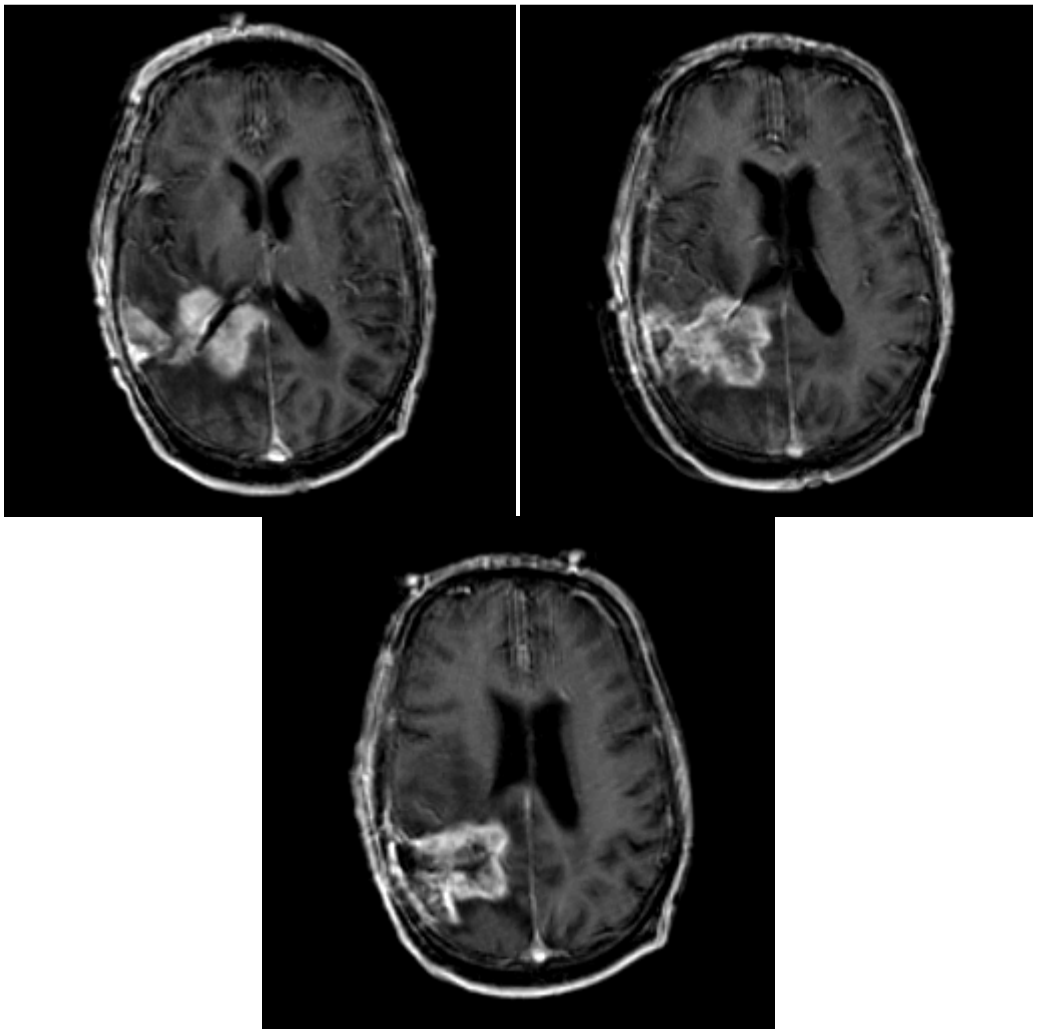

Class 2:

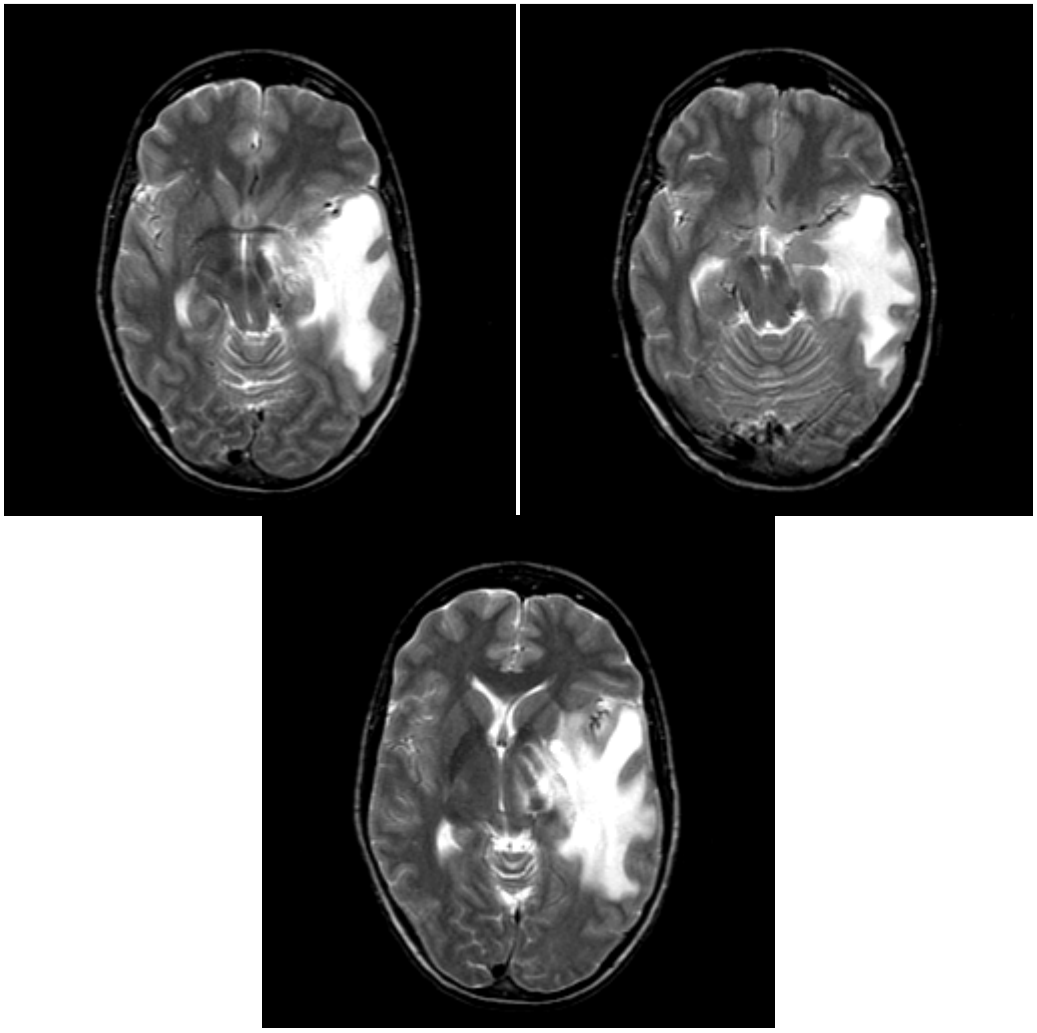

Class3:

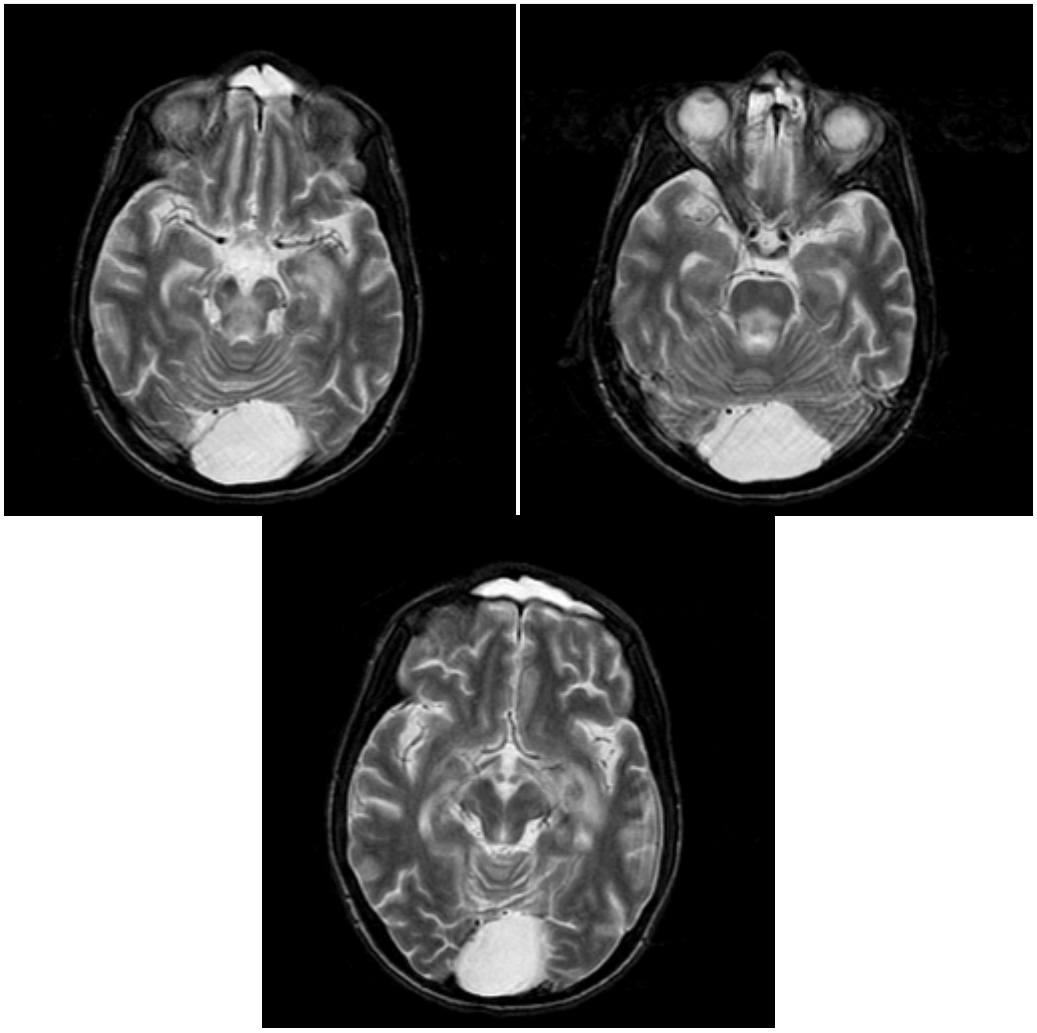

Class4:

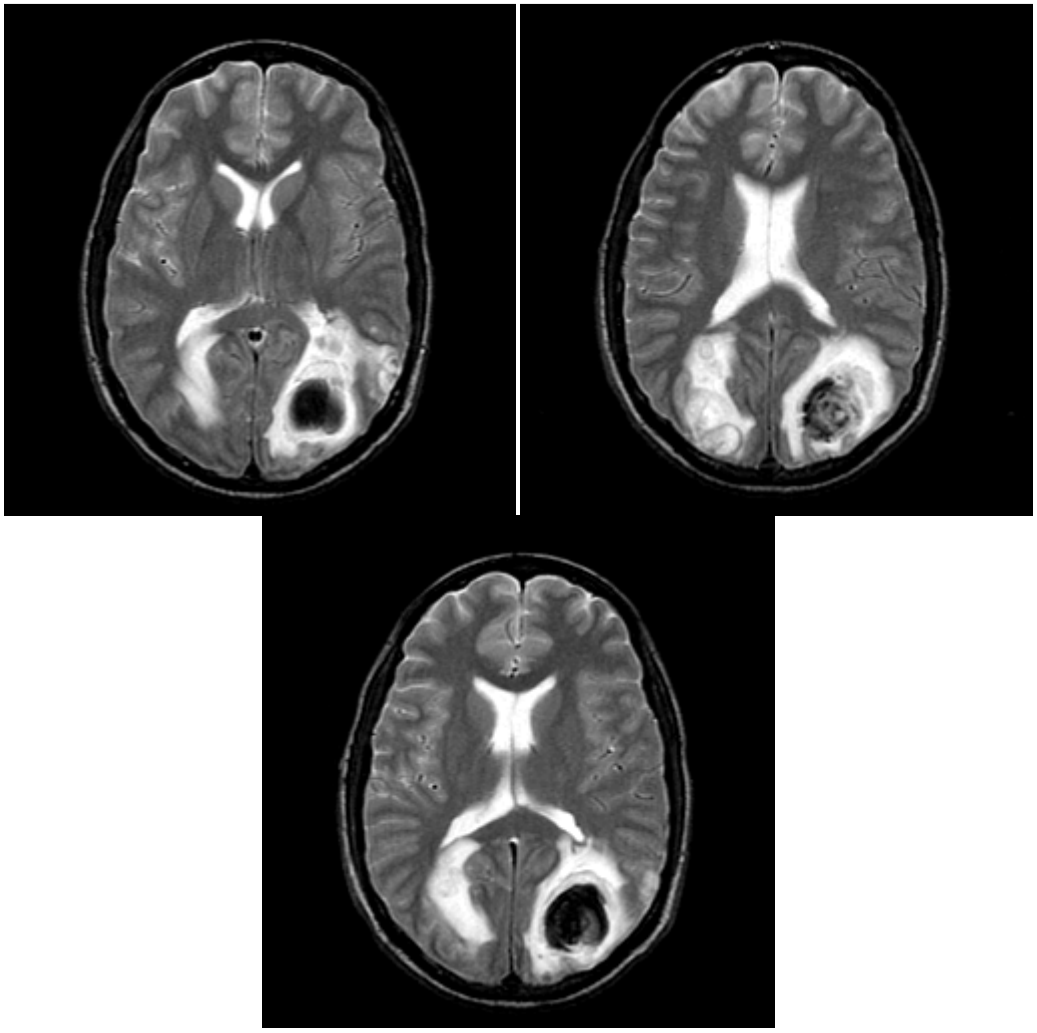

Class5:

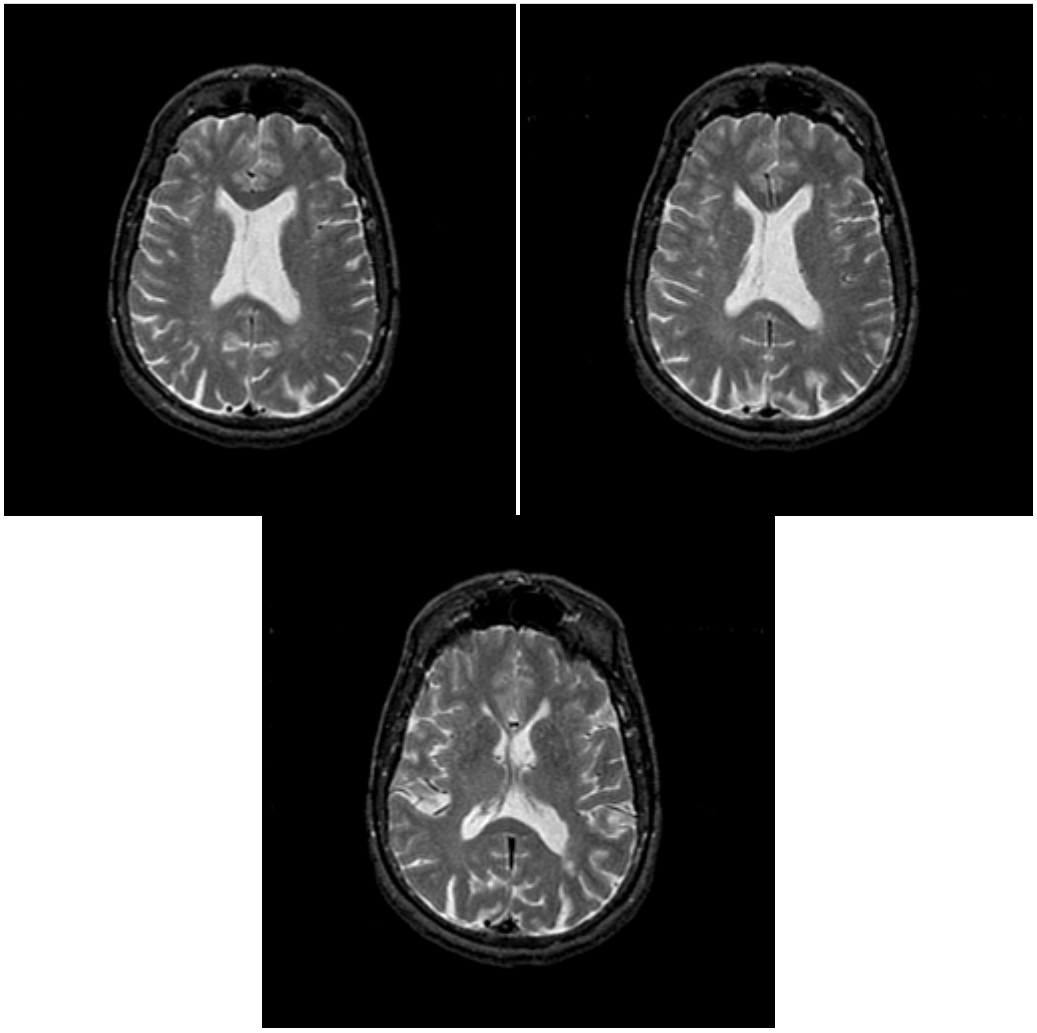

Test Data:

Class 1:

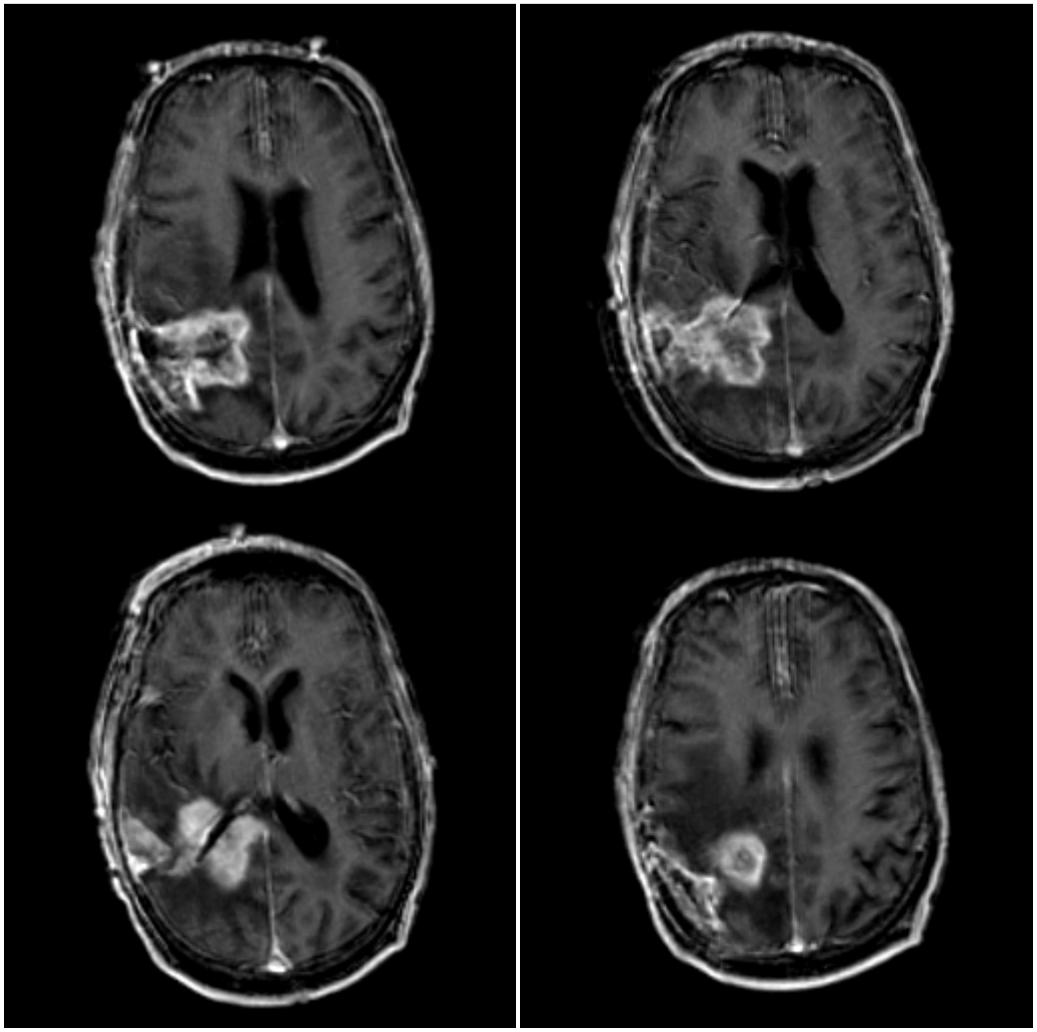

Class 2:

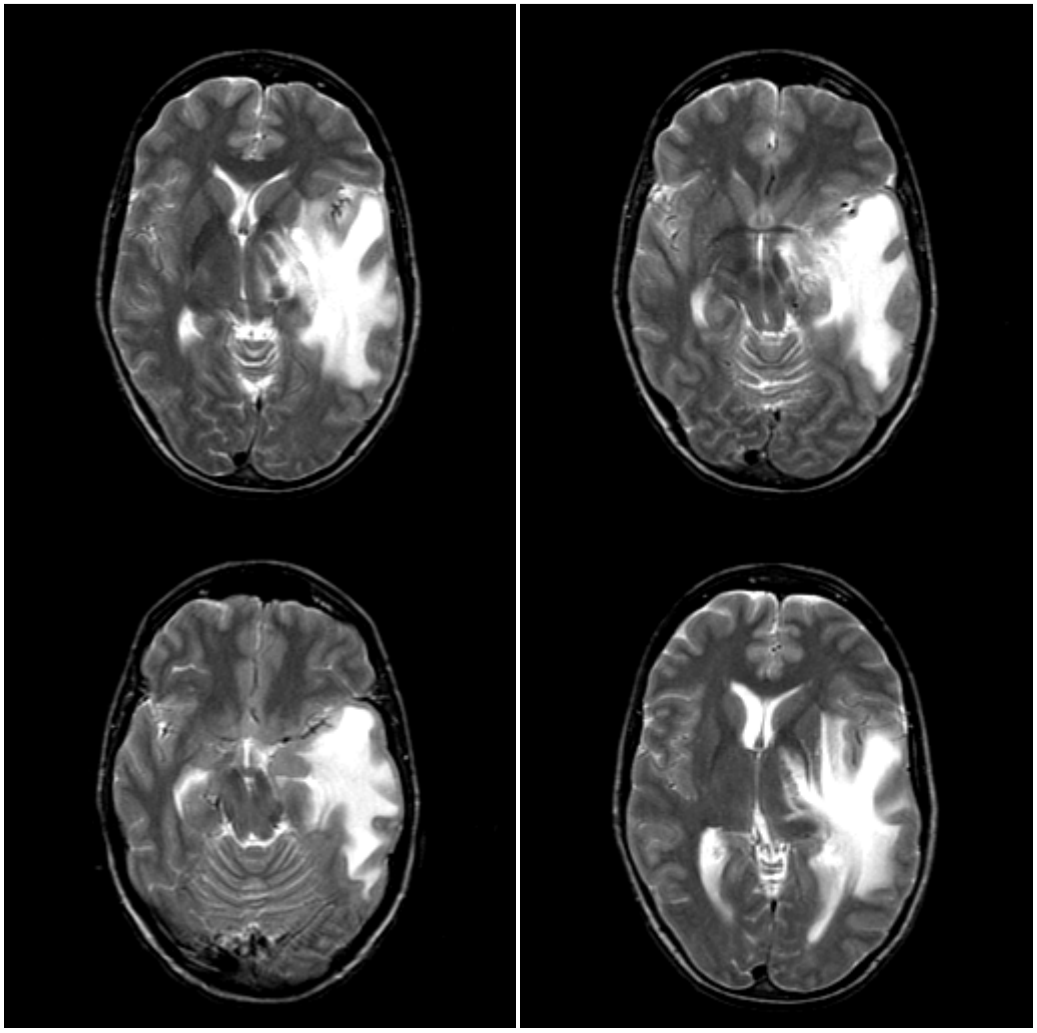

Class 3:

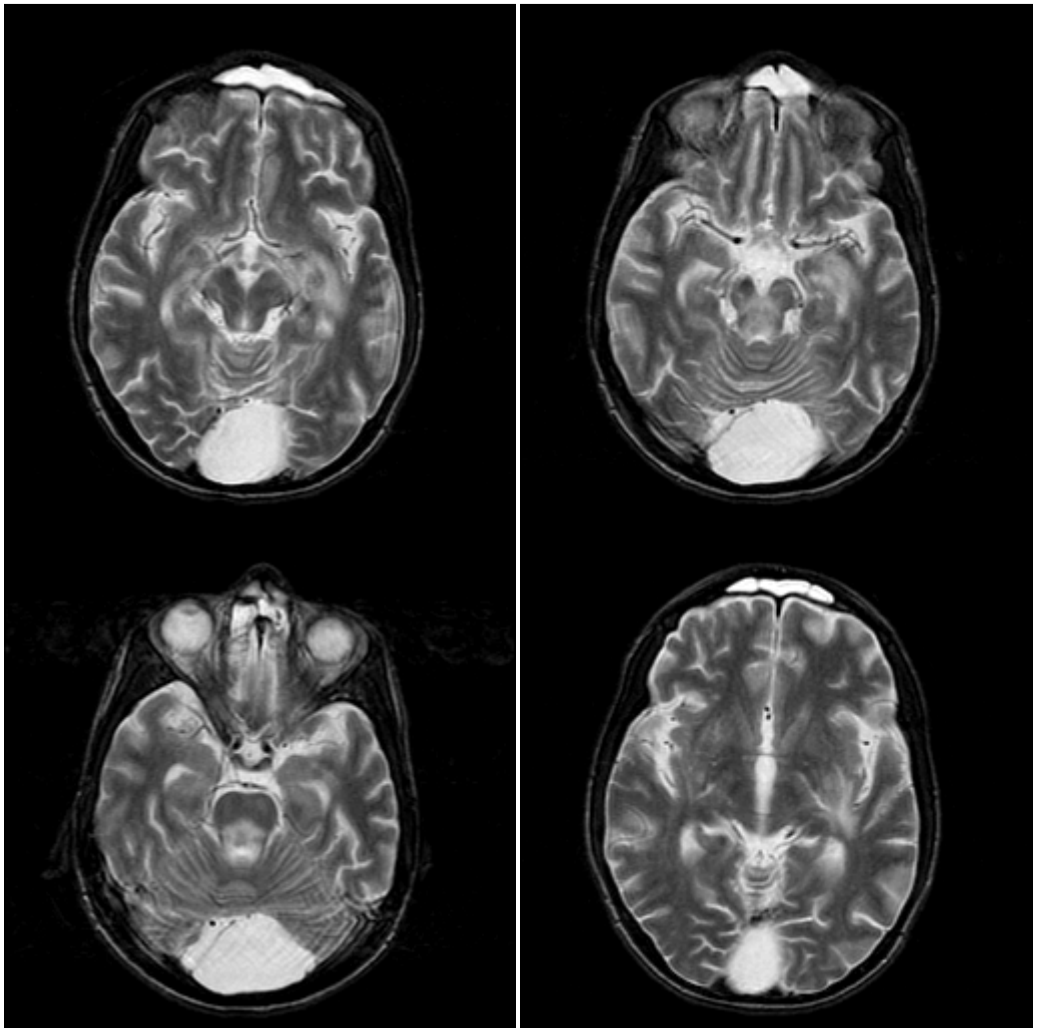

Class 4:

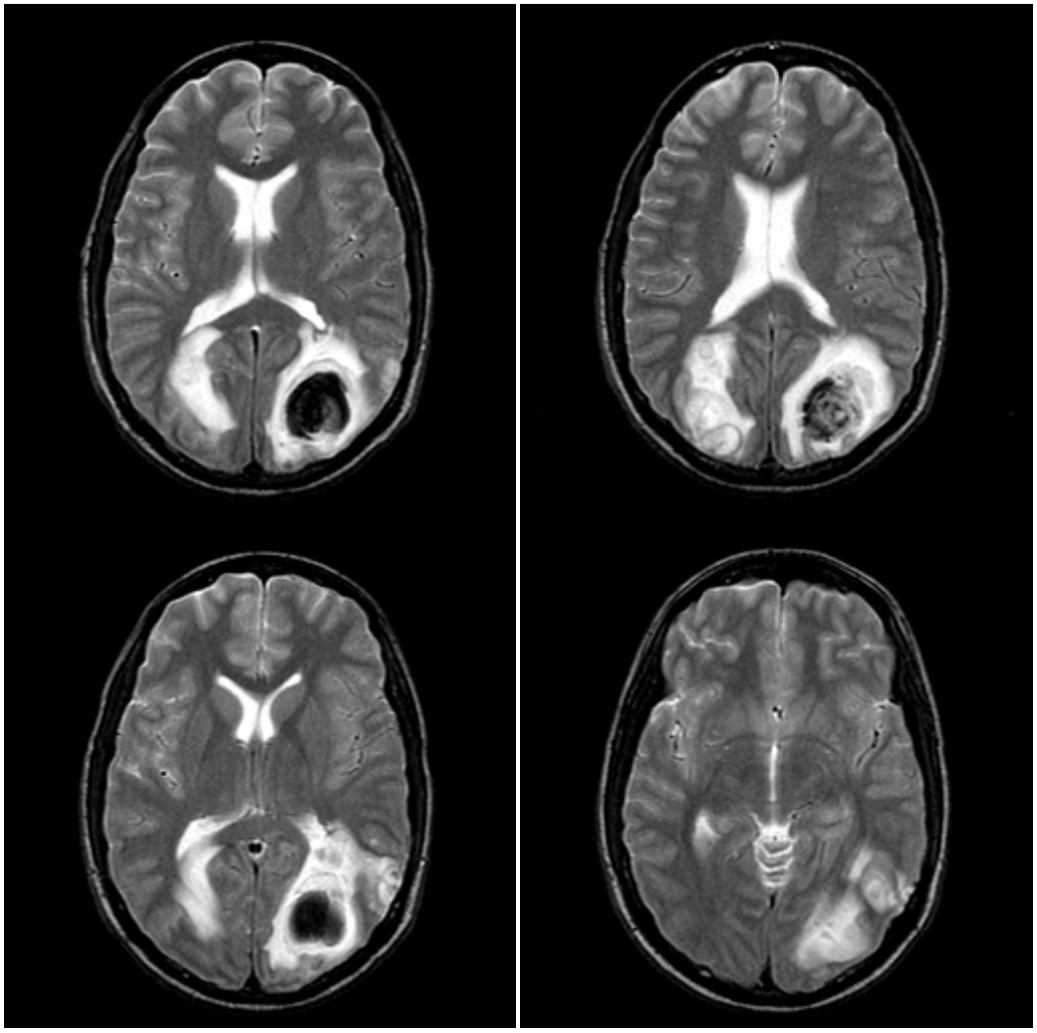

Class 5:

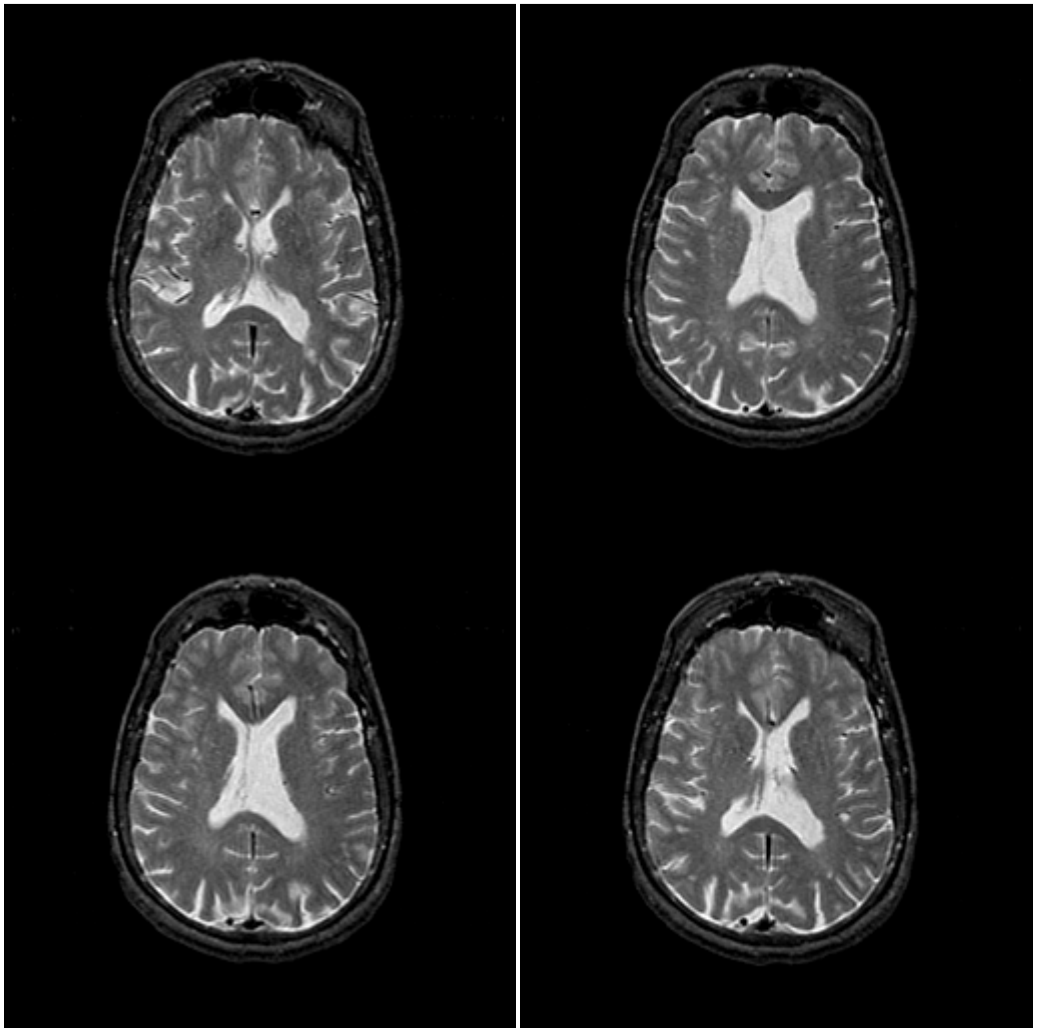

Results: Our method classify different type of tumor images correctly. Due to lack of data base it seems that all results are correct. If we apply our method on large data set results may be true up to 98% to 99%.

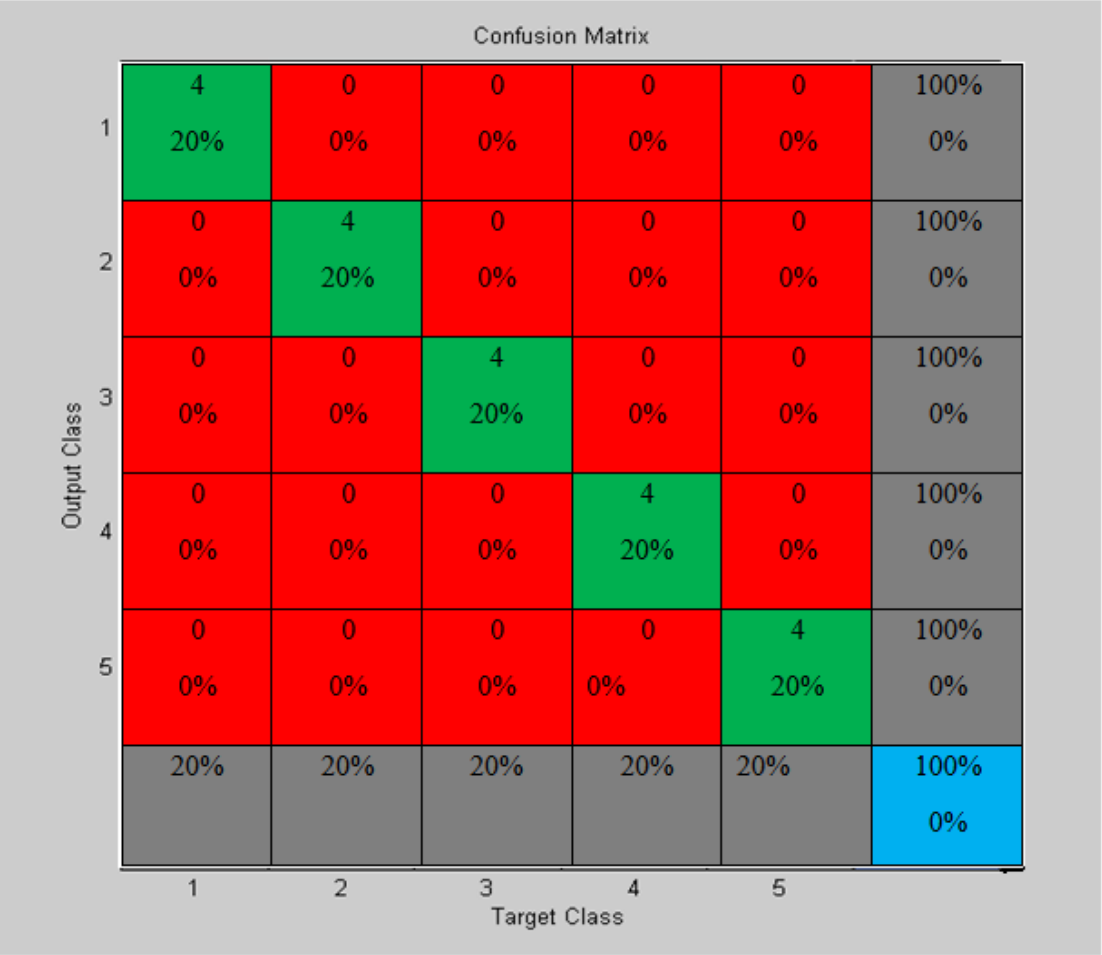

Fig.6.10 Confusion matrix of results

6.5 Conclusions

As our method provides reliable and fast detection of different types of brain tumors. Therefore it can be used in fully automated systems for tumor detection as reliable and fast detection and classification of brain tumors is of major technical and economical importance for the doctors because the information obtained will influence the treatment a patient will receive. The designed system is an efficient system for Detection and Classification of Brain Cancer from a given MRI image of cancer affected patients.

BIBLIOGRAPHY

[1]. Cancer mortality in India: a nationally representative survey

[2]. Spectrum of pediatric brain tumors in India: a multi-institutional study.

[3]. Buxton, R. B. (2002). Introduction to functional magnetic resonance imaging: Principles and techniques. Cambridge: Cambridge University Press.

[4]. Hashemi, R. H., Bradley, W. G., & Lisanti, C. J. (2004). MRI the basics. (2nd ed.) Philadelphia: Lippincott Williams & Wilkins.

[5]. Horowitz, A. L. (1995). MRI physics for radiologists. (3rd ed.) New York: Springer-Verlag.

[6].Jezzard, P. & Smith, S. (2001). Functional MRI: an introduction to methods.

[7]. Standard Operating Procedure for IMAGEN SOP-06/10/2008 WP2: fMRI tasks

[8]. Frackowiak, R. S. J., Friston, K. J., Frith, C. D., Dolan, R. J., & Mazziotta, J. C. (1997). Human brain function. San Diego: Academic Press.

[9]. Functional Neuroradiology: Principles and Clinical Applications Scott H. Faro, Feroze B. Mohamed, Meng Law

[10].Daniel Gembris ,Correlation analysis on GPU systems using NVIDIA's CUDA 9 May 2009 / Accepted: 25 May 2010 / Published online: 17 June 2010_ Springer-Verlag 2010

[11]. Jonathan Wolpaw, Elizabeth Winter Wolpaw Brain-Computer Interfaces: Principles and Practice New York: Oxford University Press Inc.

[12] . S. Chaplot, L.M. Patnaik, N.R. Jagannathan, Classification of magnetic resonance brain images using wavelets as input to support vector machine and neural network, Biomed. Signal Process. Control 1 (2006) 86–92

[13] . S. Kara, F. Dirgenali, A system to diagnose atherosclerosis via wavelet transforms, principal component analysis and artificial neural networks,Expert Syst. Appl. 32 (2007) 632–640

[14]. M. Maitra, A. Chatterjee, Hybrid multiresolution Slantlet transform and fuzzy c-means clustering approach for normal-pathological brain MR image segregation, Med. Eng. Phys. (2007), doi:10.1016/j.medengphy.2007.06.009.

[15]. S. Mallat “A wavelet tour to signal processing”

[16]. These images were collected from the Harvard Medical School website http:// med.harvard.edu/AANLIB/